Acta Astronautica 237 (2025) 159–173

Contents lists available at ScienceDirect

Acta Astronautica

journal homepage: www.elsevier.com/locate/actaastro

Research paper

Short-term response of cerebrovascular and ocular hemodynamics from micro- to hyper-gravity: A multiscale mathematical analysis

Francesco Tripoli [a,*], Luca Ridolfi [b,c], Stefania Scarsoglio [a,c]

[a] Department of Mechanical and Aerospace Engineering, Politecnico di Torino, Corso Duca degli Abruzzi 24, Turin, 10129, Italy
[b] Department of Environmental, Land and Infrastructure Engineering, Politecnico di Torino, Corso Duca degli Abruzzi 24, Turin, 10129, Italy
[c] PolitoBioMed Lab, Politecnico di Torino, Corso Duca degli Abruzzi 24, Turin, 10129, Italy

ARTICLE INFO

Keywords:
Space medicine
Spaceflight associated neuro-ocular syndrome
Cardiovascular modeling
Cerebro-ocular hemodynamics
Micro-gravity
Hyper-gravity

ABSTRACT

Exposure to micro- and hyper-gravity characterizes the spaceflight environment, leading to several short- to long-term physiological alterations. However, both acute and long-term cerebrovascular and ocular responses are still being investigated and far from being understood, with experimental data being fragmented and incongruent.

In this study, we aim to shed light on cerebro-ocular hemodynamics during short-term exposure to altered gravitational acceleration (from $0g$ to $3g$), by employing a multiscale 0D-1D model of the cardiovascular system. The modeling approach consists of a 1D representation of the arterial and coronary circulations, along with a 0D parametrization of the arteriolar, capillary, venous, cardiopulmonary, coronary, and cerebro-ocular circulations. The model is equipped with short-term regulation mechanisms (i.e., cerebral autoregulation, baroreceptors, and cardiopulmonary reflex) and includes the collapse of the neck veins.

After validating the model against experimental measurements of cerebral and ocular hemodynamic parameters, our findings indicate that micro-gravity leads to increased cerebral and ocular perfusion pressure (CPP and OPP, respectively), whereas beat-averaged values of cerebral blood flow (CBF) are near-constant due to cerebral autoregulation. However, pulsatile values of pressure and flow rate are increased, especially in the distal cerebral circulation. Additionally, the equilibrium between intracranial and intraocular pressure (ICP and IOP, respectively), which is thought to play an important role in the onset of Spaceflight Associated Neuro-Ocular Syndrome, is disrupted, resulting in reduced translaminar pressure (TLP). Conversely, hyper-gravity induces significant orthostatic stress that results in a reduction of CPP and OPP. Consequently, CBF abruptly drops at higher g values, together with hemodynamic pulsatility. In these conditions, ICP decreases more than IOP, leading to an increase in TLP.

Present results further underline the usefulness of numerical methods in the comprehension of the pathophysiological mechanisms that occur during exposure to altered gravity conditions, where clinical measurements are rare and difficult to obtain.

1. Introduction

Changes from supine to standing posture or gravitational acceleration transitions from micro- to hyper-gravity alter the hydrostatic gradient of blood pressure along the longitudinal axis (z-axis) of the body [1,2], resulting in a different blood volume distribution across the cardiovascular system. Specifically, the gradual removal of the hydrostatic pressure gradient in the hypo-gravity range [$0g$–$1g$] up to its complete absence along the z-axis in the supine posture and weightlessness condition ($0g$) elicits a fluid shift towards the thoracic and cranial regions [3–6], whereas the upright posture and hyper-gravity condition (higher than $1g$) induce a fluid redistribution towards the lower limbs [1,7,8].

While on Earth, cyclic postural transitions (which are comparable to gravity transitions within the hypo-gravity range) result in normal and physiological diurnal blood pressure fluctuations, human spaceflight involves prolonged exposure to a gravitational environment that differs significantly from the terrestrial one. In particular, the combination of extended periods of micro-gravity and brief intervals of hyper-gravity (typically encountered during launch or re-entry phases) places the cardiovascular system in an altered and extreme environment. As a

* Corresponding author.
E-mail address: francesco.tripoli@polito.it (F. Tripoli).

https://doi.org/10.1016/j.actaastro.2025.08.028
Received 12 June 2025; Received in revised form 13 August 2025; Accepted 14 August 2025
Available online 21 August 2025

consequence, exposure to these conditions leads to several short- and long-term physiological alterations [9–14].

In micro-gravity, apart from the well-known cardiovascular adaptations – fluid shift-induced increase in heart size, stroke volume, and cardiac output in the short-term, cardiac atrophy, total blood volume reduction, and reduced exercise tolerance in the long-term [6,15–18] –, both acute and long-term cerebrovascular and ocular responses are still being investigated and far from being understood [19,20]. Furthermore, the difficulties in acquiring clinical data in the cerebral and ocular regions, combined with the absence of a standardized experimental protocol and the limited number of studies, result in fragmented and incongruent data [19]. Nevertheless, recent studies revealed an association between micro-gravity-induced cerebrovascular alterations and the so-called Spaceflight Associated Neuro-Ocular Syndrome (SANS) [21–28]. This important syndrome, classified by NASA as one of the major risks for human spaceflight [29], consists of specific neuro-ocular anomalies, including optic disk edema, globe flattening, choroidal and retinal folds, and other ocular structural changes [21,30]. To date, although the pathogenesis of SANS remains unclear, elevated intracranial pressure (ICP) due to micro-gravity-induced headward fluid shift is thought to be the main driver of the syndrome [6,25,31–33]. In addition, other studies hypothesized that the interplay between intraocular pressure (IOP) and ICP could play a major role in the onset of SANS [22,32,34,35].

In hyper-gravity, the overall picture is even more problematic. The primary challenge lies in accurately replicating these conditions. In fact, while certain aspects of micro-gravity can be simulated through ground-based analogs, such as head-down bed rest (HDBR) or dry immersion [36,37], hyper-gravity can only be reproduced by means of human centrifuges and parabolic flights [38–40]. In these conditions, due to the very short duration and intrinsic complexity of these experiments, accurately measuring cerebral and ocular hemodynamic parameters can be even more challenging than acquiring them in micro-gravity. As a result, clinical measurements of ICP and IOP in hyper-gravity conditions are currently lacking, and only limited data on cerebral blood flow [41,42] and oxygenation are reported in the literature [43]. Furthermore, in the context of space travel, although some studies have reported a reduction in cerebral blood flow during human centrifuge experiments [44,45], it has been hypothesized that intermittent exposure to mild levels of hyper-gravity could mitigate physiological deconditioning [46–48].

Given the above difficulties in characterizing the cerebral hemodynamics, cardiovascular numerical modeling represents a promising method for investigating complex physiological mechanisms, such as those governing cerebral and ocular circulations during exposure to micro- and hyper-gravity environments. Previous studies have already demonstrated that the numerical approach can be an effective tool for investigating the cardiovascular system under different postures and gravity conditions [49–54]. Following this computational approach, in the present study, we aim to shed light on the cerebrovascular and ocular hemodynamics during altered gravitational acceleration by employing a multiscale 0D-1D model of the cardiovascular system. Specifically, we investigate the steady-state short-term response of the cerebral and ocular circulations to gravity transitions from $0g$ to $3g$ in the upright posture. To the best of our knowledge, no studies in the literature have systematically investigated cerebral hemodynamics across such a broad spectrum of gravitational acceleration.

Our 0D-1D multiscale cardiovascular model was recently validated against experimental data of the most significant central cardiac parameters in the gravity range [$0g$-$3g$] [55]. Here, we further validate the model by comparing our results with measured data reported in the literature by focusing on cerebral blood flow velocity, cerebral perfusion pressure, intracranial pressure, and intraocular pressure.

Our study investigates the cerebral and ocular responses to gravity changes by describing both the proximal and distal cerebral circulation in terms of pressures and flow rates, paying attention to the distribution of the blood across the anterior and posterior cerebral circulations as gravitational acceleration varies, and highlighting the interaction between ICP, IOP, and the arterial pressure at the eye level, in an effort to better comprehend their role in neuro-vestibular dysfunctions.

2. Methods

In this section, we first outline the key elements of the multiscale 0D-1D model of the cardiovascular system. Subsequently, details about numerical simulations and how gravity and posture changes were simulated are presented.

2.1. Mathematical model

The multiscale model is closed-loop and its architecture consists of a 1D representation of the arterial and coronary circulations, together with a 0D parametrization of the arteriolar, capillary, venous, cardiopulmonary, coronary, and cerebro-ocular circulations [54]. To reproduce the acute response, the model is equipped with short-term regulation mechanisms – i.e., cerebral autoregulation, baroreceptors, and cardiopulmonary reflex – and includes the collapse of the neck veins and the resulting decoupling between intracranial and systemic venous regions [55–57]. The model was recently validated against experimental data measured during parabolic flight and human centrifuge studies focusing on the main central hemodynamic parameters: heart rate, arterial blood pressure, stroke volume, and cardiac output [55]. In the an overview of the central hemodynamics validation is recalled and summarized in Fig. A.6. Validation of the 0D cerebro-ocular model is instead presented and discussed in Section 3.1. A fully detailed description of the model equations and parameter settings is provided in the Supplementary Material together with a scheme of the entire model, while Fig. 1 shows details of the 1D arterial tree upper region (left side of Fig. 1) coupled with the lumped-parameter model of the cerebrovascular and ocular circulations (right side of Fig. 1).

2.1.1. Central-systemic circulation

The 1D arterial tree includes a network of 63 arteries (48 main large arteries and 15 coronary arteries) modeled as straight and tapered vessels. To describe blood motion, we exploit the 1D axisymmetric form of the Navier–Stokes equations for mass and momentum balance, by assuming a circular cross-section, a flat-parabolic flow profile, and blood as a Newtonian fluid with constant density and viscosity ($\rho = 1050$ kg/m^3 and $\mu = 4 \cdot 10^{-3}$ Pa $\cdot$ s). The gravitational acceleration is directly included as an external forcing field within the momentum balance equation, paying attention to the arteries' orientation with respect to both the frontal axis and the horizontal plane. Mechanical and viscoelastic properties of the arterial walls are modeled through a non-linear constitutive equation linking the arterial blood pressure with the cross-sectional area [54].

The inlet of the 1D model of the arterial tree (the ascending aorta) is coupled with the 0D model of the aortic valve, whereas the outlets of the main arteries (with the exception of the 1D coronary, internal carotid and vertebral arteries) are linked with several three-element RLC Windkessel models of the 0D arteriolar compartment via a characteristic impedance Z_c [54]. Each element of the Windkessel model describes a specific property of a vascular compartment, with R, L, and C indicating the hydraulic resistance, the blood inertia, and the vessel compliance, respectively. The arteriolar compartments are then merged into five body regions, describing the peripheral circulation in the arms, upper abdomen, lower abdomen, legs, and extracranial district (depicted on the top of Fig. 1 and perfused by the left and right external carotid arteries, ECA). Each of these regions includes an RLC model of the capillary, venular, and venous compartments. Three additional RLC compartments, describing the superior, inferior, and abdominal tracts of the vena cava, are enclosed to link the venous

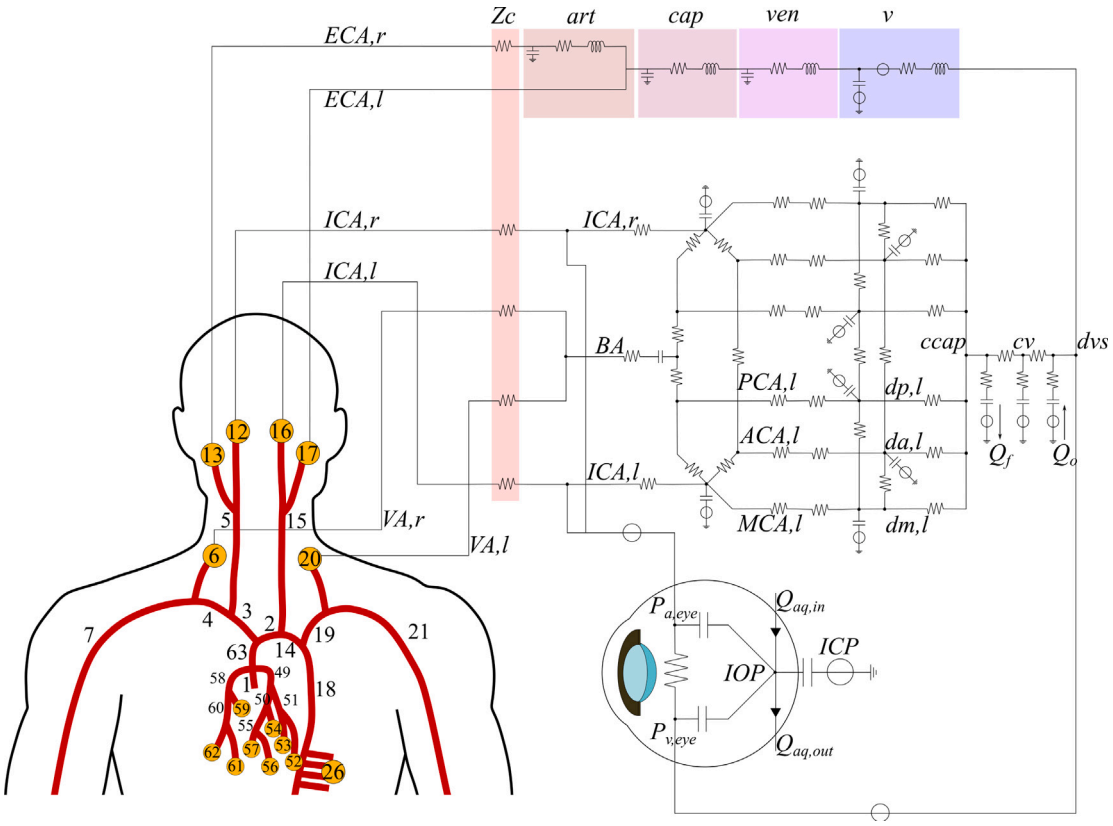

Fig. 1. Schematic representation of the 0D-1D model with a focus on the cerebral and ocular lumped-parameters model. The 1D arterial tree (sketched on the left in red, with black numbers referring to 1D main arterial vessels) is linked to the 0D model of the extra-cranial, cerebral, and ocular circulations via characteristic impedances Z_c. ECA,r and ECA,l denote the right and left external carotid arteries, whereas *art*, *cap*, *ven*, and *v* indicate the 0D compartments (arteriolar, capillary, venular, and venous, respectively) of the extra-cranial circulation. ICA,r, ICA,l, VA,r, and VA,l represent the right and left internal carotid arteries and the left and right vertebral arteries (which converge into the basilar artery, BA). ACA,l, MCA,l, and PCA,l indicate the left anterior, middle, posterior cerebral arteries, whereas *da*, *dm*, and *dl* represent the distal anterior, middle, and posterior arteries, respectively. Cerebral capillaries, cerebral veins, and dural venous sinus are denoted by *ccap*, *cv*, and *dvs*, respectively. Q_f and Q_o are the cerebrospinal fluid formation and outflow rates, respectively. ICP and IOP denote the intracranial and ocular pressures, whereas $P_{a,eye}$, $P_{v,eye}$, $Q_{aq,in}$, and $Q_{aq,out}$ indicate the arterial and venous pressure at the level of the eye and the aqueous humor inflow and outflow rates, respectively. (For interpretation of the references to color in this figure legend, the reader is referred to the web version of this article.)

compartments with the right atrium. Furthermore, two different non-linear pressure–volume relationships are implemented to model the non-linear effects of distending leg veins volume [54] and venous collapse of neck veins (additional details are reported in the Supplementary material), whereas venous valves are added within the arm and leg venous compartments to prevent reverse blood flow. Finally, to account for the gravitational force, a pressure generator modeling the hydrostatic component of the pressure is inserted within each venous compartment (including the three vena cava compartments) according to Stevino's law [54], considering both the blood specific weight ρg and the anatomical extension of each compartment.

The 0D model of the cardiopulmonary circulation includes the description of the four cardiac chambers, together with a lumped-parameter model of the pulmonary circulation. Cardiac valves are modeled as non-ideal diodes, whereas the cardiac contractility is described employing time-varying elastances. To model the pulmonary circulation, a two-element RC model is adopted to represent the arterial and venous pulmonary compartments. All the compartments of the cardiopulmonary circulation are subjected to intrathoracic pressure (ITP), which varies with both the body position and gravitational force [58].

The 1D extremities of the coronary arteries are connected to several 0D models of the microvascular coronary circulation. Each of these models is subdivided into three branches corresponding to a specific layer of the myocardium (subepicardium, midwall, and subendocardium). To represent the external compression exerted by the heart during ventricular contraction, each myocardial layer is subjected to the intramyocardial pressure (IMP), which is assumed to act as an extravascular pressure [58].

Short-term regulation mechanisms governed by the autonomic nervous system (i.e., the baroreceptors and cardiopulmonary reflex) are implemented to maintain the system's homeostasis. The sympathetic and parasympathetic activities are computed employing a sigmoid function, which depends on the variations of a sensing variable with respect to its target value. For the baroreflex mechanism, the sensing variable is the average between the pressures in the aortic arch and the left/right carotid sinus over a cardiac cycle, whereas the averaged right atrial pressure is selected for the cardiopulmonary reflex. The baroreflex controls the heart rate (chronotropic effect) and the strength of contraction in both ventricles (inotropic effect), together with the vascular tone of the systemic vasculature (arteriolar and capillary resistances, venous and venular unstressed volumes, and venous and venular compliances). Conversely, the cardiopulmonary reflex regulates only peripheral resistances and venous tone.

2.1.2. Cerebrovascular and ocular circulations

The right side of Fig. 1 focuses on the architecture of the 0D model of the cerebral and ocular circulations. Specifically, the 1D internal carotid and vertebral arteries are coupled with the lumped parameter model of the cerebrovascular and ocular circulations, whereas the 1D outlets of the external carotid arteries are connected to the 0D extracranial circulation.

A network of interconnected resistances and compliances describing the key features of cerebral physiology is employed to model the cerebrovascular circulation [54]. In particular, the Circle of Willis is modeled as a closed ring composed of several resistances mimicking the pre-communicating portions of the anterior and posterior cerebral arteries (ACAs and PCAs), as well as the anterior and posterior communicating arteries (ACoA and PCoA). From the Circle of Willis, the six main cerebral arteries – i.e., the middle cerebral arteries (MCAs), the post-communicating portion of the ACAs and PCAs – branch out, distally arranging in six distinct vascular beds, which model the pial arterial and cerebral arteriolar circulations. To maintain adequate cerebral blood flow (CBF), the compliances and hydraulic resistances of each vascular bed are governed by the cerebral autoregulation mechanism. Downstream of the cerebral arteriolar circulation, CBF converges into the post-capillary circulation, which is modeled as a unique pathway from cerebral capillaries to dural venous sinuses. Additionally, the processes of cerebrospinal fluid formation and absorption are modeled through resistive components, while the intracranial pressure (ICP) is computed by applying the mass preservation and assuming a non-linear pressure–volume relationship for the craniospinal system (additional details are provided in the Supplementary Material). Finally, the outflow of the cerebrovascular model is directly connected to the superior vena cava compartment.

The lumped-parameter model of the ocular circulation is described by means of six different compartments, which govern the dynamics of both the intraocular pressure (IOP) and ocular globe volume (V_g) [54]. Specifically, the aqueous humor compartment regulates the IOP via the inflow and outflow of the aqueous humor fluid within the eye globe. The retrobulbar subarachnoid space (rSAS) accounts for the external influence of ICP on IOP by means of the compliance C_{rg}. Subsequently, three compartments are used to model the arterial, capillary, and venous circulation of the eye. Finally, a passive and isovolumic compartment is added to model the lens and the vitreous humor.

2.2. Numerical simulations

Our mathematical model was employed to investigate the acute steady-state response of the cerebrovascular and ocular circulations to gravity changes in the range [0g-3g] in a standing posture. Therefore, a head-up tilt test at 1g (which is our baseline reference) was first simulated in order to obtain the steady-state response in the upright position, by applying the following function to model the time-dependent variation of the tilt angle α:

$$\alpha(t) = \begin{cases} 0, & \text{if } t < t^{I}_{start} \\ \dfrac{\alpha_{tilt}}{2} \cdot \left[1 - \cos\left(\dfrac{t - t^{I}_{start}}{T_{tilt}} \cdot \pi\right)\right] & \text{if } t^{I}_{start} < t < t^{I}_{start} + T_{tilt} \\ \alpha_{tilt} & \text{if } t > t^{I}_{start} + T_{tilt}, \end{cases} \quad (1)$$

where α_{tilt}, t^{I}_{start}, and T_{tilt} indicates the final angle reached after the tilt (90° for the upright posture), the tilting starting time, and the tilting period in which the posture change occurred (T_{tilt} = 22.5 s), respectively. After obtaining the standing 1g steady-state condition, gravity transitions from 1g up to the desired level of gravity were imposed by the cosinusoidal function:

$$\frac{g(t)}{g_0} = \begin{cases} 1 & \text{if } t < t^{II}_{start} \\ 1 + \dfrac{1}{2} \cdot \left[\left(\dfrac{g}{g_0}\right)_f - 1\right] \cdot \left[1 - \cos\left(\dfrac{t - t^{II}_{start}}{T_g} \cdot \pi\right)\right] & \text{if } t^{II}_{start} < t < t^{II}_{start} + T_g \\ \left(\dfrac{g}{g_0}\right)_f & \text{if } t > t^{II}_{start} + T_g, \end{cases} \quad (2)$$

where $(g/g_0)_f$, t^{II}_{start}, and T_g denoted the final level of gravitational acceleration reached after the transition, the transition starting time, and the transition duration, respectively. Both t^{I}_{start} and t^{II}_{start} were chosen to ensure that any initial transients from model initialization were fully extinguished. Furthermore, a fixed gravity rate of $\pm 0.01 g/s$ was applied across all simulations to avoid numerical instabilities. Although this gravity rate may not be representative of that typically encountered in real-life applications, our study was focused on the short-term steady-state condition, which a previous study [58] demonstrated to be independent of both the gravity rate and tilting rate.

Finally, the 1D governing equations were discretized and solved numerically by a Discontinuous Galerkin Finite Elements method. Time integration of both 0D and 1D equations was performed employing a 2-step Runge–Kutta explicit scheme with a constant time step. In total, 31 simulations were carried out, covering a gravity range from micro- (0g) to hyper-gravity (3g).

3. Results

The following section is divided into three subsections: in the first one, the comparison between the 0D-1D cerebral-cardiovascular model outcomes and experimental data reported in the literature is discussed, in order to validate the 0D cerebro-ocular model. In the second and third subsections, the short-term response of cerebrovascular and ocular hemodynamics to gravity changes are investigated, respectively.

3.1. Validation of the cerebrovascular and ocular models

Our multiscale mathematical model was previously validated in a recent study [55] that investigated the cardiac function under micro- and hyper-gravity conditions by comparing the behavior of six central hemodynamic variables – heart rate, cardiac output, stroke volume, mean arterial pressure, systolic arterial pressure, and diastolic arterial pressure – with experimental data extracted from parabolic flight and centrifuge studies (for further details, please refer to).

Here, to further validate our mathematical framework focusing on the cerebro-ocular 0D model, we evaluated the model outcomes against experimental measurements of cerebral blood flow velocity ($CBFV$), cerebral perfusion pressure (CPP), intracranial pressure (ICP), and intraocular pressure (IOP). Due to the difficulty in obtaining relevant measured data from the literature under hyper- and micro-gravity spaceflight conditions, we considered experimental data from parabolic flight [34,41,59], human centrifuge [44,45], and tilt test studies [23,34,44,54,57,59,60]. It is important to note that, due to the limitations of the acquisition methodologies [61,62], ICP and IOP measurements are currently unavailable in the hyper-gravity environment. Therefore, in the experimental studies considered to construct the validation dataset, ICP and IOP were only detected at 1g and during terrestrial analogs of the micro-gravity environment (supine and head down tilt postures at 1g and micro-gravity phase of parabolic flights). Conversely, the considered experimental studies provided measurements of $CBFV$ and CPP in both micro- and hyper-gravity conditions. Specifically, $CBFV$ and CPP (typically defined as the difference between the mean arterial pressure at the cerebral level and ICP) were experimentally estimated as the cerebral blood flow velocity and the mean arterial pressure at the middle cerebral artery level, respectively.

In order to minimize inter-study variability – arising primarily from the lack of a standardized experimental protocol and differences in the characteristics of the subject groups (i.e., sample size, age range, fitness levels, and number of female/male subjects) – each cerebro-ocular parameter was referred to the 1g condition (denoted as g_0). Specifically, CPP and $CBFV$ measurements were divided by their respective 1g values, while ICP and IOP were normalized by subtracting the corresponding 1g values. Subsequently, the experimental data were pooled for each variable across each gravity level according to the following relationships [63]:

$$\mu^{p}_{X_j} = \frac{\sum_{i=1}^{k} n_i \mu_{X_{i,j}}}{\sum_{i=1}^{k} n_i} \quad (3)$$

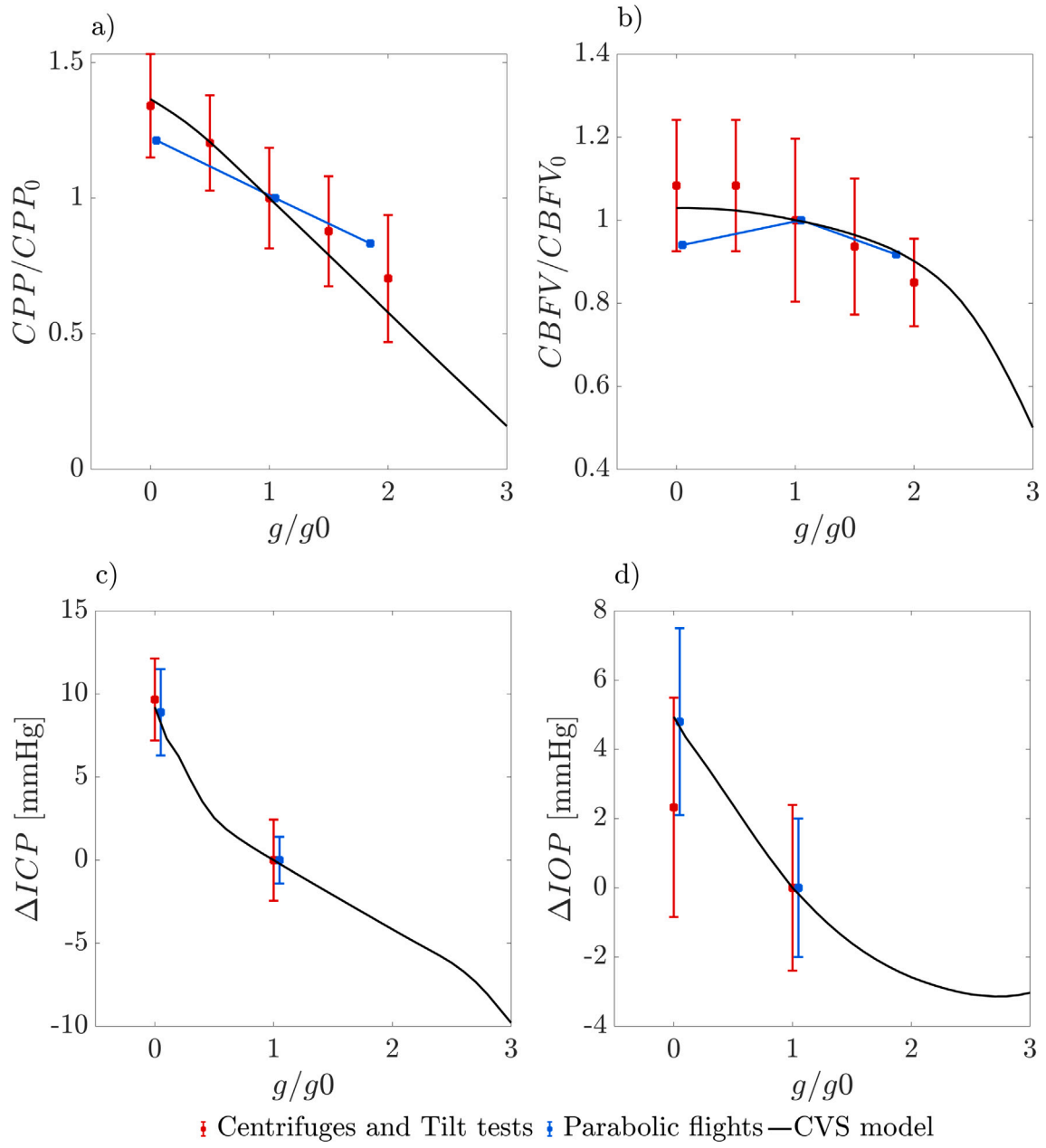

Fig. 2. Pooled mean and standard deviation values (μ^p_{Xj} and σ^p_{Xj}) are depicted with red (centrifuges and tilt tests data) and blue (parabolic flight data) points and lines, whereas model outcomes are depicted with black solid curves. Panels (a-d) show the normalized values of CPP, $CBFV$, ICP, and IOP, respectively. (For interpretation of the references to color in this figure legend, the reader is referred to the web version of this article.)

$$\sigma^p_{Xj} = \sqrt{\frac{\sum_{i=1}^{k} \sigma^2_{Xi,j}(n_i - 1) + \sum_{i=1}^{k} n_i(\mu_{Xi,j} - \mu^p_{Xj})^2}{\sum_{i=1}^{k} n_i - 1}} \quad (4)$$

where n_i, $\mu_{Xi,j}$, and $\sigma_{Xi,j}$ indicate the number of subjects recruited in the ith literature study, and the mean and standard deviation for the Xth cerebro-ocular variable at the jth gravity level, respectively.

In Fig. 2, the pooled mean (μ^p_{Xj}) and standard deviation (σ^p_{Xj}) values from the centrifuge and tilt test studies (red lines), as well as those from parabolic flights (blue lines), are shown along with the model outcomes (black curves) in the gravity range [0g-3g]. Experimental data from centrifuge and tilt test studies were pooled together, as centrifuges were specifically employed to investigate the cerebral response in hyper-gravity, whereas tilt tests were conducted to evaluate the micro-gravity environment.

As depicted in Fig. 2a, changes in gravity significantly affect the hydrostatic term of the cerebral arterial pressure, leading to a monotonic decrease in cerebral perfusion pressure as gravity increases. Specifically, tilt test and centrifuge measures show a reduction of −47.5% in μ^p_{CPP} at 2g with respect to 0g, whereas μ^p_{CPP} decreases by −31.3% as gravity grows from 0g to 1.8g during parabolic flight. Conversely, cerebral blood flow velocity (see Fig. 2b) is regulated by cerebral autoregulation, which maintains a near-constant cerebral blood flow when CPP is between 50 mmHg and 150 mmHg [64,65]. As evidence of this mechanism, tilt test and centrifuge data reveal a slight increase in μ^p_{CBFV} (+8.3% from 1g to 0g) when entering the hypo-gravity range, whereas at 2g, due to the decreased CPP, a -15% decline is detected. Parabolic flight measures [41] show a slight decrease as gravitational acceleration varies from 1g to 0g. However, it should be noted that in parabolic flights, the micro-gravity phase lasts only a few seconds (approximately 20 s) and occurs after the first hyper-gravity

phase, during which a −8.2% decline is observed with respect to the normo-gravity condition.

Focusing on the ICP (Fig. 2c) response to gravity changes, both tilt test measurements and parabolic flight data [23,34,57] exhibit close agreement, with ICP increasing by approximately 10 mmHg in both conditions ($\mu^p_{\Delta ICP}$ rises by +9.7 mmHg and +8.9 mmHg at $0g$ during tilt tests and parabolic flight, respectively). Finally, experimental data indicate that micro-gravity elicits an increase in IOP. However, this increase is lower than that observed in ICP. Specifically, according to tilt test data, $\mu^p_{\Delta IOP}$ rises by +2.3 mmHg at $0g$, whereas parabolic flight measurements report an elevation of +4.8 mmHg.

The results of our cardiovascular model (black curves in Fig. 2) are in good agreement with the experimental data, with all the model outcomes being within the range $\mu^p_{X_j} \pm \sigma^p_{X_j}$. Notably, the model is able to reproduce the impact of the gravity-dependent hydrostatic term on the cerebral perfusion pressure, as well as the cerebral autoregulation mechanism. In fact, $CBFV$ (Fig. 2b) – which was computed as the flow rate in the middle cerebral artery divided by its lumen area – is near-constant within the hypo-gravity range, whereas beyond this range it starts to decrease in line with the centrifuge and parabolic flight data. Additionally, our model effectively replicates the micro-gravity-induced increase in ICP and IOP, also detecting the non-linear trend of ICP, which was already observed in a previous study of head-up tilt test and associated with the collapse of the jugular veins [57]. Further comments on the behavior of these variables will be provided in the following sections, considering their potential physiological implications in the context of cerebral (see Section 3.2) and ocular (see Section 3.3) responses to gravity changes.

3.2. Cerebrovascular response to gravity changes

In order to describe the cerebrovascular response to gravitational force variations, Fig. 3 shows an overview of cerebral pressures and flow rates in relation to gravitational acceleration along a proximal-to-distal pathway including the internal carotid artery (ICA), the proximal and distal middle cerebral artery (MCA and dm, respectively), the cerebral capillary region ($ccap$), the cerebral venous compartment (cv), and the dural venous sinuses (dvs). Pressure and flow rate means ($\overline{P}$ and $\overline{Q}$) and pulsatile values ($\Delta P = P_{max} - P_{min}$ and $\Delta Q = Q_{max} - Q_{min}$) are reported for each vascular district. In addition, intracranial pressure (ICP) and cerebral blood flow (CBF) are shown.

The ICA (Fig. 3a) and the MCA (Fig. 3b) hemodynamics exhibits a similar behavior. Both mean arterial pressures decrease significantly – by 71.1 mmHg and 70.7 mmHg (−87.9% and −88.3%), respectively – as gravity rises from $0g$ to $3g$. This decline follows an almost linear trend due to the gravity-dependent hydrostatic component of the pressure. Specifically, since at the heart level the mean arterial pressure (MAP) slightly increases within the hypo-gravity range due to the baroreceptor reflex [55], both $\overline{P}_{ICA}$ and $\overline{P}_{MCA}$ exhibit a modest downward concavity in the range [$0g$-$1g$]. Beyond this range, MAP remains nearly constant, and the hydrostatic term, which is linearly dependent on g, becomes the only factor responsible for the pressure drop. It is worth noting that, at higher g values, the considerable increase in the hydrostatic contribution results in a significant reduction of CPP, which drops below the functioning range of the cerebral autoregulation, compromising CBF and suggesting that these extreme conditions are incompatible with continued consciousness. Additionally, pulsatile pressure ΔP (shaded area in Fig. 3a and b) also diminishes in the ICA and MCA as gravity varies from $0g$ to $3g$, with reductions of 27.5 mmHg (−69.2%) and 27.4 mmHg (−70.7%), respectively. This reduction is due to the different responses between systolic and diastolic arterial pressure when gravity increases. During the hyper-gravity range, a contraction in the amplitude of the pressure waveform (with a decrease in the systolic pressure and an increase in the diastolic one) is observed at the central level, resulting from a reduced stroke volume and increased heart rate [55]. Due to the cerebral autoregulation mechanisms, the reduction in flow rate within the ICA and the MCA is limited to less than 10% up to $1.6g$ and $1.8g$, respectively. After these values, the cerebral autoregulation loses the capability of counteracting pressure drop, leading to a greater decrease in the mean flow rate, equal to −52.0% in the ICA and −51.4% in the MCA at $3g$ (variations are referred to the $0g$ condition). Interestingly, the behavior of pulsatility ΔQ differs from that of ΔP, ΔQ remaining nearly constant throughout the gravity range with variations limited to $\pm 10\%$ with respect to g_0 (−10% and +10% towards hyper- and micro-gravity conditions, respectively).

Moving towards the distal circulation (Fig. 3c), the pressure behavior does not vary: both $\overline{P}_{dm}$ and ΔP_{dm} decrease as gravity increases. Similar to the flow rate in the MCA, the cerebral autoregulation maintains a near-constant $\overline{Q}_{dm}$ up to $1.8g$ (−8.91% from $0g$ to $1.8g$), whereas a reduction of −50.9% is detected at $3g$. Instead, differently to proximal circulation, ΔQ_{dm} largely varies with gravity changes. In particular, pulsatile values of Q_{dm} decrease by up to −88.7% at $3g$ with respect to the $0g$ condition. A comparable pattern was observed in a previous work [66], where an increase in pulsatile values variations in the proximal-to-distal direction was found during $0g$ (positive variations) and $1.8g$ (negative variations) parabolic flight phases, both relative to the $1g$ phase. This amplifying behavior of the pulsatile values in the distal cerebral circulation is attributable to the complex combination of resistances and compliances that characterize the deep cerebral circulation [67]. In fact, the intricate interplay between the mechanical properties (compliances and resistances) of the different cerebral hemodynamic compartments (in series or in parallel with each other) results in heightened temporal inertia of the deep cerebral circulation. Therefore, the increased (in micro-gravity) and reduced (in hyper-gravity) pulsatility at the central level [55] is further amplified and damped within the distal cerebral circulation, respectively.

In the capillary and venous compartments (Fig. 3d), $\overline{P}_{ccap}$ and $\overline{P}_{cv}$ exhibit a clear non-linear behavior as gravity increases, and both curves show a distinct slope variation in the proximity of $0.5g$. This variation is closely related to ICP (Fig. 3e), which in turn is affected by changes in the hydrostatic pressure term. According to the hypothesis that the hydrostatic gradients in the venous system mainly control ICP and the collapse of the neck veins hydrostatically disconnects intracranial and venous system regions [57], only the distance between the most cranial region of the collapsed vein and the dural venous sinuses contributes to the hydrostatic pressure term. This collapse-induced decoupling mechanism explains the slope variation observed in $\overline{P}_{ccap}$ and $\overline{P}_{cv}$, suggesting that the collapse of the neck veins occurs in the proximity of $0.5g$. With regard to ΔP_{ccap} and ΔP_{cv}, they both decrease as gravitational acceleration changes from $0g$ to $3g$ (−78.0% and −59.5% at $3g$ with respect to the $0g$ condition, respectively), thus confirming the reduced cerebral pulsatility at higher g values.

As shown in Fig. 3e, the pressure in the dural venous sinuses ($\overline{P}_{dvs}$) varies similarly to ICP, yet ΔP_{dvs} decreases abruptly after venous collapse. In addition, by focusing on the mean flow rate in the cerebral venous district ($\overline{Q}_{cv}$, see Fig. 3d) and $\overline{CBF}$ (Fig. 3e), variations within −10% are observed when g reaches values up to $2.1g$. Beyond this value, both parameters decrease by −39.3% at $3g$ (with respect to $0g$). It should be noted that this variation is smaller than the one observed in the MCA and dm districts (−51.4% and −50.9%, respectively). Finally, consistent with the observations made at the distal circulation level (dm), both ΔQ_{cv} and ΔCBF are greatly affected by gravity changes, diminishing by −87.0% and by −95.4% from $0g$ to $3g$, respectively.

To explain the different behavior between $\overline{CBF}$ and $\overline{Q}_{MCA}$, Fig. 4 displays the fractions of cerebral blood flow (f_i) in various cerebral vascular districts. Starting from the arteries entering the brain (ICA and basilar artery, BA), up to the distal cerebral regions downstream the Circle of Willis – i.e., the distal anterior, the distal middle, and the distal posterior cerebral regions (da, dm, and dp) –, we studied how the distribution of blood flow across these regions changes with gravity. In particular, the fraction of cerebral blood flow in the ith regions f_i is

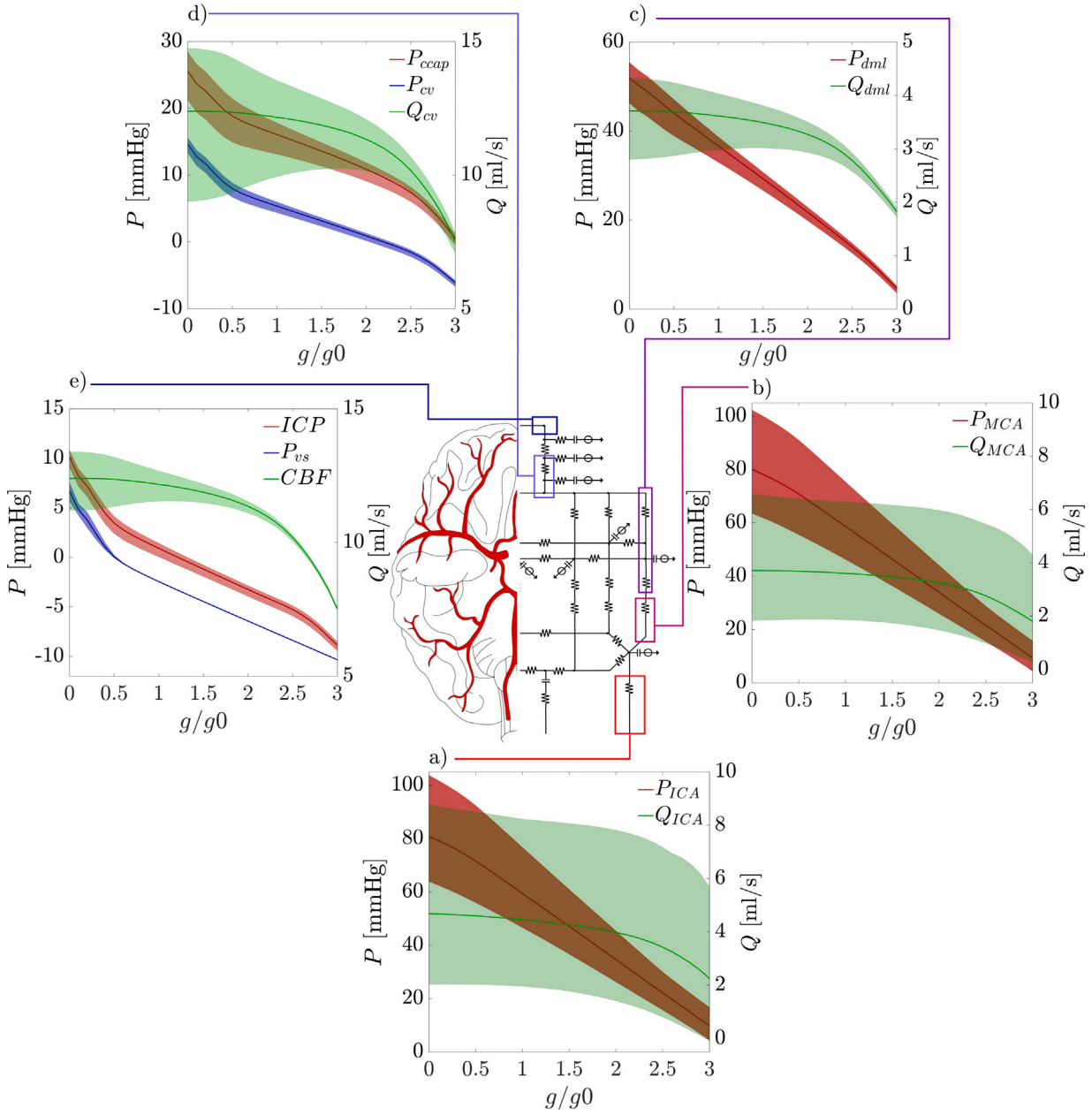

Fig. 3. Mean values (solid lines) and amplitudes (shaded area) of pressure and flow rate responses to gravity changes along the left ICA-MCA pathway: (a) pressure and flow rate in the internal carotid artery (ICA); (b) pressure and flow rate in the middle cerebral artery (MCA); (c) pressure and flow rate in the distal middle arterial district (dm); (d) pressure and flow rate in the cerebral capillaries and cerebral veins ($ccap$ and cv); (e) pressure in the dural venous sinuses (dvs), intracranial pressure (ICP), and cerebral blood flow (CBF).

defined as $f_i = \overline{Q}_i/\overline{CBF}$, where $\overline{Q}_i$ denotes the mean flow rate within the ith cerebral vascular district of interest and $\overline{CBF}$ indicates the mean cerebral blood flow. We focused on the left side of the cerebral circulation due to the symmetry of the cerebral lumped parameters model. The only marginal difference between the two cerebral hemispheres lies in the inlet conditions of the left and right internal carotid arteries: both $ICAs$ originate from the common carotid arteries ($CCAs$), but the left CCA arises from the aortic arch, while the right CCA stems from the brachiocephalic trunk.

Fig. 4a shows that f_{ICA} and f_{BA} exhibit opposite responses to gravity changes. In fact, as gravity varies from $0g$ to $3g$, f_{ICA} decreases from 37.8% to 29.9%, while f_{BA} rises from 23.8% to 40.4%. Additionally, beyond $2.5g$, f_{BA} becomes larger than f_{ICA}, indicating that during hyper-gravity conditions, the anterior cerebral circulation experiences a greater cerebral blood flow decrease with respect to the posterior circulation. This behavior is primarily due to the reduced pressure drop within the BA (−79.9% from $0g$ to $3g$) compared to that within the ICA (−87.9%).

Recalling that the distal anterior and middle regions of the brain are primarily perfused by the ICA (which branches into the anterior and middle cerebral arteries) and that the distal posterior cerebral region is mainly supplied by the BA (which branches into the left and right posterior cerebral arteries), similar findings to the ICA-BA partition can also be observed for the distal cerebral circulation. In particular, Fig. 4b depicts the fraction of CBF within each district of the distal circulation (da, dm and dp, respectively). Similarly to f_{ICA}, at higher g values f_{dm} decreases from 29.7% at $1g$ to 24.2% at $3g$, while f_{da} is almost constant around 8% throughout the investigated gravity range. Conversely, a non-linear increase in f_{dp} (from 12.2% to 16.9%) is detected as g varies from $1g$ to $3g$. Therefore, the different responses observed between the

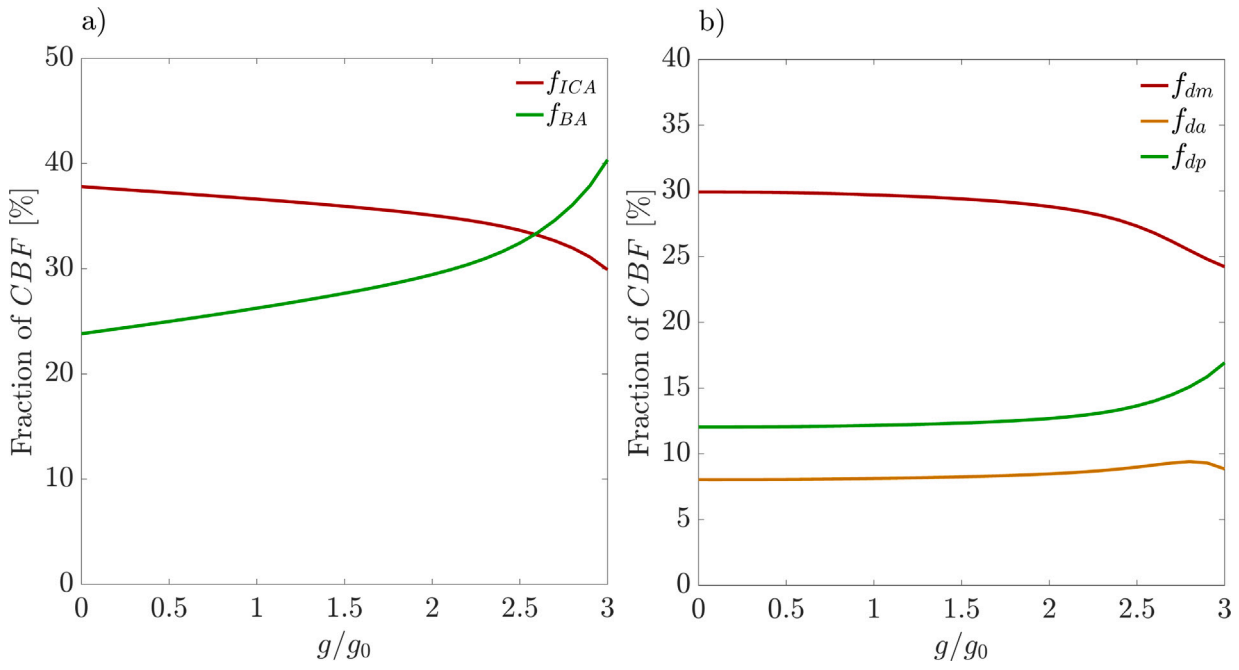

Fig. 4. Gravity-dependent blood flow distribution in the cerebral districts. Curves indicate the fraction of cerebral blood flow f_i, which is defined as $f_i = \overline{Q}_i/\overline{CBF}$ (where i = ICA, BA, da, dm, and dp), as the gravitational acceleration varies.

anterior and posterior cerebral circulations could explain the greater decrease previously detected in Q_{MCA} with respect to CBF (see Fig. 3b and e). In fact, the posterior circulation compensates for the larger decrease in Q_{ICA} and Q_{MCA}, thus limiting the total CBF reduction at higher g values.

3.3. Ocular response to gravity changes

To describe the response of the ocular system to gravity changes, Fig. 5 shows the main parameters depicting the ocular hemodynamics: the mean and pulsatile values of the intraocular pressure (IOP), the translaminar pressure (TLP), the ocular perfusion pressure (OPP), and the arterial and venous pressure at the eye level ($P_{a,eye}$ and $P_{v,eye}$).

Fig. 5a highlights that the eye arterial pressure ($P_{a,eye}$) exhibits an equivalent behavior to P_{ICA}. In fact, $\overline{P}_{a,eye}$ and $\Delta P_{a,eye}$ decrease by 84.0% and 35.4% as g grows from $0g$ to $3g$. The same figure shows that, from micro- to hyper-gravity, the mean eye venous pressure ($\overline{P}_{v,eye}$) drops from 6.7 mmHg at $0g$ to −1 mmHg at $3g$ (−114.9%), thus reaching negative values, whereas $\Delta P_{v,eye}$ decreases by −41.2% as gravity increases from $0g$ to $3g$.

Fig. 5b and c focus on the translaminar pressure (defined as the difference between IOP and ICP), intraocular pressure, and ocular perfusion pressure (computed as the difference between $P_{a,eye}$ and IOP). In recent years, astronautical interest and research in the g-dependence of these pressures has grown significantly as it has been associated with the onset of SANS [25,32,34]. Figs. 3e and 5b show that, due to the headward fluid shift (driven by the gradual removal of the hydrostatic pressure gradient), both mean intracranial pressure, $\overline{ICP}$, and mean intraocular pressure, $\overline{IOP}$, increase during exposure to micro-gravity with respect to the $1g$ condition. In particular, $\overline{ICP}$ rises from 0.9 mmHg (at $1g$) to 10.1 mmHg (at $0g$), while $\overline{IOP}$ increases from 13.6 mmHg (at $1g$) to 18.5 mmHg (at $0g$). These results align with the ICP values observed in head-down tilt test studies and IOP measurements conducted in the micro-gravity environment (as highlighted in Fig. 2 of the validation Section 3.1 [23,34,54,57,59,60]). As a consequence, mean TLP ($\overline{TLP}$) decreases from 12.7 mmHg to 8.4 mmHg as the gravity varies from $1g$ to $0g$ (−33.7%). In particular, notice that $\overline{TLP}$ abruptly decreases when the gravitational acceleration is less than $0.5g$, due to the non-linear behavior of ICP (see Fig. 3e). Due to the increased pulsatility detected in the distal cerebral circulation, ΔICP increases by +27.2% (from 1.37 mmHg at $1g$ to 1.74 mmHg at $0g$) during exposure to micro-gravity, whereas ΔIOP rises from 3.80 mmHg to 5.24 mmHg (+37.9% from $1g$ to $0g$). As a consequence of the heightened pulsatility of both ICP and IOP, ΔTLP also increases, varying from 3.76 mmHg at $1g$ to 5.20 mmHg at $0g$ (+38.1%).

Conversely, $\overline{ICP}$ decreases up to −8.9 mmHg at $3g$, whereas $\overline{IOP}$ appears to converge towards a plateau value around 10.5 mmHg, with $\overline{IOP}$ showing a non-linear relationship as function of g (Fig. 5b). In particular, the rate of decrease in IOP diminishes as g increases, exhibiting a convex shape. This non-linear trend is associated with the response of $P_{v,eye}$, which, as depicted in Fig. 5a, exhibits a similar non-linear evolution to that of IOP. In fact, following the same approach as Nelson et al. [68], where the episcleral venous pressure (EVP) is equal to $P_{v,eye}$, in the steady state $\overline{IOP}$ depends only on EVP, the aqueous humor formation rate and the uveoscleral outflow rate (see Eq. 51 of the Supplementary Material). As a consequence, the translaminar pressure (recall that $TLP = IOP - ICP$) increases non-linearly within the hyper-gravity range, as the rate of decrease in IOP differs from that of ICP, with $\overline{TLP}$ varying from 12.7 mmHg to 19.4 mmHg at $3g$ (+53.3% with respect to the $1g$ value). Thus, as gravity acceleration grows, the increase in $\overline{TLP}$ becomes more dependent on the changes in ICP. Additionally, as a result of the general drop in the amplitude values across the cerebral circulation at higher g values, both ΔICP and ΔIOP decrease by −32.6% and −57.9% as gravity increases from $1g$ to $3g$, respectively. Consequently, ΔTLP also decreases, varying by −47.3% in the range [$1g$-$3g$].

As a consequence of the increased mean and pulsatile arterial blood pressure in the eye ($P_{a,eye}$) at $0g$, mean OPP ($\overline{OPP}$) rises from 55.8 mmHg at $1g$ to 72.8 mmHg at $0g$ (+30.6%), while ΔOPP increases from 50.7 mmHg at $1g$ to 59.7 mmHg at $0g$ (+17.5%). Conversely, $\overline{OPP}$ and ΔOPP decrease up to 4.1 mmHg (−92.7%) and 41.0 mmHg (−19.3%) at $3g$, respectively. This drop is primarily due to the reduced $\overline{P}_{a,eye}$ and $\Delta P_{a,eye}$. In fact, $\overline{P}_{a,eye}$ decreases by −78.9% from $1g$ to $3g$, while $\overline{IOP}$ varies only by −22.3%.

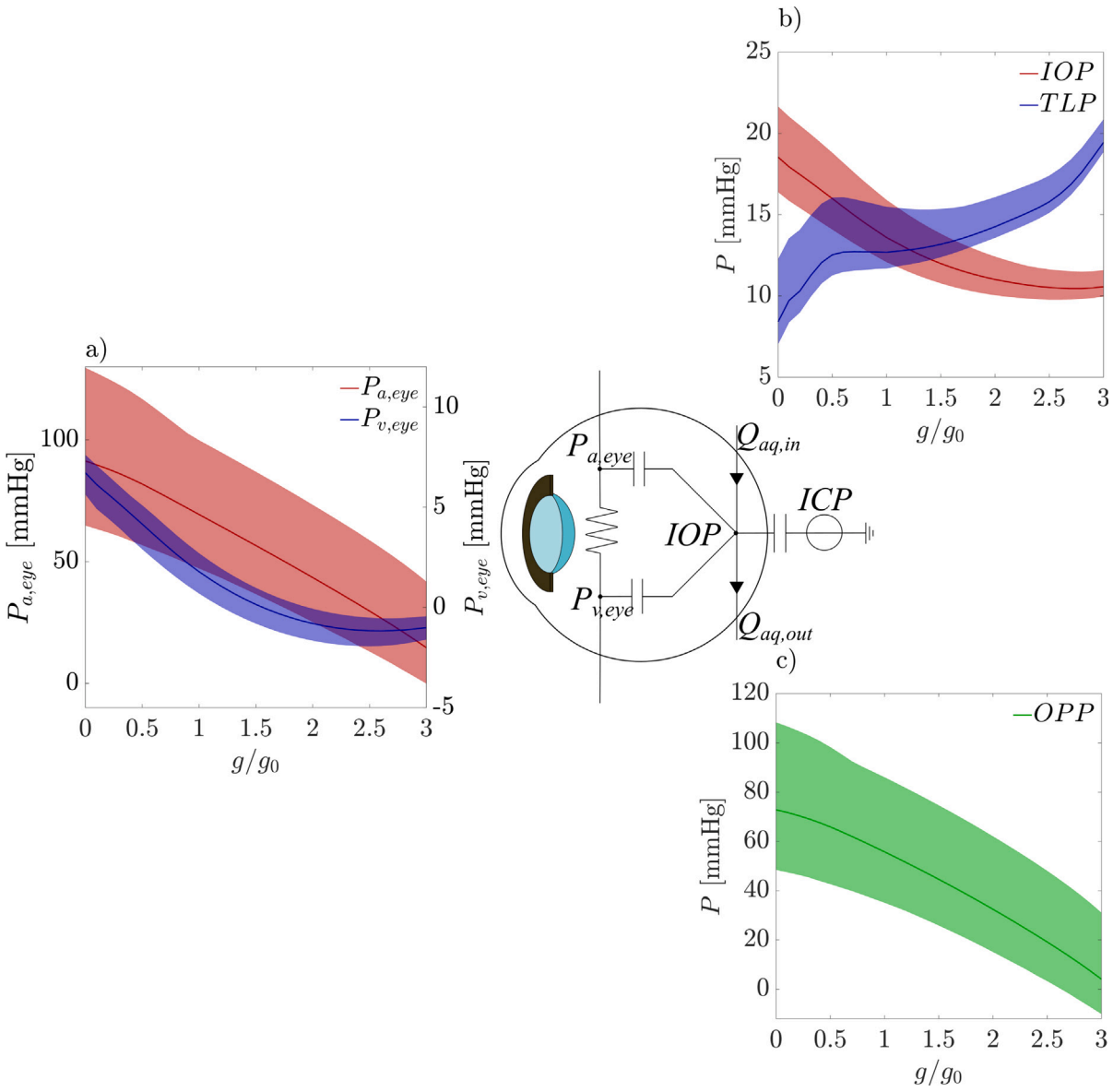

Fig. 5. Mean values (solid lines) and amplitudes (shaded area) of: (a) arterial and venous pressure at the eye level ($P_{a,eye}$ and $P_{v,eye}$); (b) the intraocular pressure (IOP) and the translaminar pressure (TLP); (c) the ocular perfusion pressure (OPP).

4. Discussion

Over the years, micro-gravity has been extensively studied, due to the effects of long-term space missions on the cardiovascular system [6,10,14,69], while hyper-gravity has received less attention due to the difficulties in reproducing this condition and its occurrence only during certain phases of spaceflight, such as launch or landing maneuvers. To the best of our knowledge, no systematic studies have been carried out on the short-term response of cerebrovascular and ocular hemodynamics in a standing posture to hypo- and hyper-gravity conditions within such a wide range of g. The mathematical framework described in this study allowed us to investigate this response, highlighting different non-linear behaviors that could be crucial in the comprehension of human adaptation to the hostile spaceflight environment.

Within the hypo-gravity range (i.e., [0g-1g] range), the reduction of the hydrostatic pressure contribution causes an increase in cerebral blood pressure. The mean arterial pressure grows by +36.1% at the left ICA as gravitational acceleration varies from 1g to 0g. Additionally, moving along the proximal-to-distal circulation, this increase becomes even more accentuated, rising by +42.0% in the middle distal district, by +59.1% in the cerebral capillaries, and by +173.1% in the cerebral veins. Besides the cerebral mean arterial pressure, the pulse pressure is also affected by the transition to a micro-gravity environment. In particular, the increased pulse pressure at the heart level during micro-gravity leads to an elevation of the pulsatile values of the pressure across the whole cerebral circulation. Notably, the mean arterial pressure in the cerebral capillaries and veins shows the same non-linear behavior exhibited by the intracranial pressure and the dural venous pressure (see Fig. 3e). The underlying mechanism behind this response is the collapse of the internal jugular veins (IJVs), which occurs when the transmural pressure approaches zero. Homlund et al. [57] suggested that the collapse triggers the generation of a section with constant pressure, where the most cranial point of this segment becomes the new reference point for intracranial venous pressure. Since the external pressure exerted by the surrounding tissues on the IJVs is almost zero [70], the intraluminal pressure within these vessels and, consequently, the pressure at the reference point becomes close to zero during the collapse. Thus, the hydrostatic component of P_{dvs} and ICP depends solely on the corresponding blood column situated above the collapsed region. Our model is able to capture this collapse-induced

non-linear behavior, which plays a crucial role in the regulation of both P_{dvs} and ICP during gravity changes.

The influence of micro-gravity on blood flow rates is primarily detectable in the pulsatile values, while beat-averaged values exhibit no significant variations due to cerebral autoregulation. This mechanism ensures adequate perfusion in all cerebral districts throughout the entire range of hypo-gravity. Furthermore, the fractions of cerebral blood flow in the cerebral districts downstream of the Circle of Willis remain substantially unchanged. Conversely, the flow rate pulsatile values rise – especially in the distal districts – due to the mechanical inertia (i.e., compliance) of the deep cerebral circulation, which amplifies the heightened pulsatility at the central aortic level [67]. Our model highlights a simultaneous increase of ΔP and ΔQ, particularly in the distal and deep cerebral districts. The heightened pulsatility is an index of increased variability. Hence, during acute exposure to micro-gravity, the cerebral circulation experiences strong pressure and flow fluctuations compared to the beat-averaged values, potentially leading to an increased risk of mechanical stress and vascular remodeling [71], and possible cognitive impairment and cerebral small vessel diseases [72].

Exposure to hyper-gravity triggers an elevation of the hydrostatic pressure term, resulting in a pressure drop in the vascular districts above the heart level. Our model predicts an 83.6% decrease in the mean arterial pressure in the ICA and a 74.1% decrease in the BA at $3g$ with respect to the $1g$ condition. As shown in Fig. 4, the different pressure drop between the ICA and BA propagates distally, causing a different blood flow repartition between the anterior and posterior cerebral circulation. This different response between the anterior and posterior cerebral circulation has already been documented in the literature. In fact, Bailey et al. [73] observed a modest increase in the posterior cerebral perfusion during the micro- to hyper-gravity transition elicited by parabolic flights. Moreover, Ogoh et al. [74] found a correlation between the reduction in ICA blood flow and the level of orthostatic stress induced by graded lower body negative pressure (LBNP), whereas blood flow in the vertebral arteries (VA) was not affected by the level of the LBNP. In line with these results, Sato et al. [75] observed the same differential response in the ICA and VA to orthostatic stress induced by head-up tilt (HUT) tests. These findings suggest a greater adaptability of the posterior cerebral circulation to tolerate high gravitational stress, which is crucial since the vertebro-basilar system supplies blood to important cerebral regions – such as the medulla oblongata, cerebellum, brain stem, thalamus and hypothalamus [76] – that play a crucial role in maintaining homeostasis, and where important cardiac and respiratory control centers are located. Additionally, it has been hypothesized that hypoperfusion in the vertebro-basilar system is associated with common presyncope symptoms, such as dizziness, vertigo, and nausea [75]. In the context of aviation and aerospace medicine, these findings can have significant implications and highlight the importance of the cerebral posterior circulation in relation to orthostatic tolerance. However, other studies [77–79] did not reveal any heterogeneity in regional blood flow during hypovolemic-induced orthostatic stress. These conflicting results in the literature may arise from differences in experimental protocols and signal acquisition. Moreover, many physiological mechanisms are involved in the regulation of cerebral blood flow, including changes in ICA and VA due to sympathetic activation, reactivity to CO_2, and changes in cerebral perfusion pressure. Since the effects of these mechanisms are not yet fully understood, additional experimental and numerical studies are essential to clarify the responses of the anterior and posterior cerebral circulations to orthostatic stress.

In addition to reducing the mean values of the pressure, hyper-gravity elicits a decrease of ΔP in all cerebral vascular districts. Conversely, ΔQ diminishes only in the distal districts, remaining unchanged in the ICA and MCA throughout the entire range of g. Moreover, as soon as CPP falls below 50 mmHg at approximately $1.5g$, cerebral blood flow becomes compromised, decreasing by −38.2% at $3g$ compared to normogravity conditions. In fact, the CBF reduction is below 5% at $1.8g$, beyond this value, the rate of decrease grows, suggesting an inability of cerebral autoregulation to maintain an adequate CBF at higher g values. Typically, a reduction in CBF of 50%–60% leads to the onset of presyncope [65]. Furthermore, previous studies [65,80,81] have speculated an impairment of dynamic cerebral autoregulation during orthostatic stress, which may contribute to cerebral hypoperfusion and, thus, orthostatic intolerance. Hence, our model could slightly underestimate the reduction in CBF, which could be even more pronounced during real exposure to hyper-gravity environments.

Finally, our study focused on the neuro-ocular system response to gravity changes, and, in particular, the interaction between ICP and IOP was investigated. In fact, several studies hypothesized that micro-gravity-induced ICP and IOP alterations are among the main factors contributing to the pathogenesis of SANS [6,25,31–33]. Therefore, understanding the influence of gravitational acceleration on ICP and IOP is indispensable for gathering a clearer picture of gravity-induced neurovestibular disorders. Our study suggests that as gravity varies from $1g$ to $0g$, ICP increases more than IOP, thus altering their interaction. In particular, TLP shows a highly non-linear response to gravity changes due to the non-linear behavior of ICP and IOP. In fact, within the range $[0.6g–1g]$, $\overline{TLP}$ remains almost constant, while the equilibrium between the ocular and intracranial compartments is mainly disrupted for gravitational values below $0.5g$ (due to the slope variation of ICP). This point is of crucial importance, since the lamina cribrosa is very sensitive to alterations in TLP and a chronic reduction of this pressure can lead to optic disk and refractive changes and optical nerve diseases, such as papilledema [22,24,31]. Additionally, a reduction of the gravitational acceleration increases both $\overline{IOP}$ and $\overline{P}_{a,eye}$, yet the elevation in IOP is negligible compared with the rise in $\overline{P}_{a,eye}$. Hence, $\overline{OPP}$ monotonically increases, modifying the perfusion of the eye and potentially leading to edema and choroidal blood flow changes [31,82].

Within the hyper-gravity range, ICP reaches largely negative values. Recalling that CPP is defined as the difference between MAP at the brain level and ICP, negative values in ICP effectively limit the CPP decrease. Ogoh et al. [83] suggested that these changes in ICP may counteract the gravity-induced changes in mean arterial pressure during mild orthostatic stress. However, the internal jugular venous collapse reduces the decline in ICP by lowering the hydrostatic gradient, limiting the compensatory role played by ICP during high orthostatic stress. The behavior of ICP within the hype-gravity range is fascinating but should be interpreted with caution. The absence of measurements in hyper-gravity prevents us from validating our results in a definitive manner. Our model predicts a monotonic decline in ICP as gravity increases, primarily due to the increased hydrostatic contribution, leading to significantly negative values of ICP. It is noteworthy that negative ICP has already been reported in the literature in patients with hydrocephalus who suffered CSF fluid overdrainage [84]. IOP also decreases as gravity increases, varying from 13.6 mmHg at $1g$ to 10.6 mmHg at $3g$ (−22.3%). In particular, the rate of decrease in IOP is not constant and decreases as g rises, gradually becoming smaller compared to that of ICP. Thus, hyper-gravity elicits an opposite response of TLP with respect to micro-gravity. This aspect is of great interest in the context of spaceflight countermeasures against cardiovascular deconditioning and SANS, as short-term exposure to hyper-gravity may counteract the ocular response observed in the micro-gravity environment. However, several studies observed that excessively low ICP could alter the configuration of the lamina cribrosa, leading to decreased retrograde axonal transport and glaucoma [22,85–88]. Moreover, the high orthostatic stress exerted by hyper-gravity leads to a decline in OPP due to reduced mean arterial pressure at the eye level, which is a well-known risk factor for glaucoma and choroidal thinning [82,89,90]. Despite this, hyper-gravity is typically experienced for only brief time intervals and is not consistently applied to the human body as with micro-gravity. Therefore, future studies are required to better comprehend whether suitable doses of hyper-gravity could mitigate the effects of

micro-gravity without inducing the negative effects elicited by exposure to hyper-gravity.

The present mathematical framework has some limiting aspects: (i) cerebral reactivity to different levels of CO_2 is not included in our model. Arterial CO_2 pressure (P_{a,CO_2}) affects cerebrovascular resistances, altering cerebral autoregulation [91]. In particular, an increase in P_{a,CO_2} elicits vasodilation, while a reduction in P_{a,CO_2} induces vasoconstriction [91]. It is well-known that orthostatic stress causes hypocapnia with hyperventilation, inducing a vasoconstrictive response [92]. Moreover, it has been observed that both IOP and ICP are influenced by CO_2 levels [23,34]. (ii) The functioning of the cerebral autoregulation is assumed to be optimal throughout the gravitational range, despite some authors observing impairment of the cerebral autoregulation during high orthostatic stress [65,80,81]. (iii) Our model does not account for long-term regulation mechanisms related to renal, hormonal activity, and transcapillary blood flow. In addition, muscular activation, which plays an important role in venous return to the heart, is not described.

5. Conclusion

The present study demonstrated that numerical modeling can be a powerful and effective tool for investigating cerebral and ocular hemodynamics in extreme environments, such as those represented by micro- and hyper-gravity. Our model was able to reproduce the response of the most common measured cerebral and ocular parameters ($CBFV$, CPP, ICP, and IOP) and provided insightful details that current acquisition methods are not able to detect. In particular, micro-gravity elicited an increase in the cerebral perfusion pressure due to the removal of the hydrostatic gradient. Despite this increase, the cerebral autoregulation mechanism ensured a near-constant CBF across the entire hypo-gravity range. However, pulsatile values of pressure and flow rate were increased due to heightened pulsatility at the central level. Additionally, our model revealed several non-linear gravity-dependent trends, among which those of IOP and ICP were the most significant. Specifically, our study showed that their equilibrium was mainly disrupted within the range [0g–0.5g], with the translaminar pressure being greatly reduced during acute exposure to micro-gravity, thus suggesting that it is sufficient to replicate gravity conditions similar to that between 0.6g and 1g to restore a physiological balance between ICP and IOP. Conversely, hyper-gravity induced a significant decline in cerebral blood pressure, which was responsible for both the reduction in CBF and OPP at higher g values, whereas TLP was found to increase. Thus, hyper-gravity induced an opposite response to that of micro-gravity, confirming the hypothesis that intermittent exposure to mild levels of hyper-gravity could mitigate physiological deconditioning [46–48].

In the context of space travel, these findings confirm the usefulness of numerical methods in the comprehension of the pathophysiological mechanisms that occur during exposure to altered gravity conditions, such as those inducing SANS and cardiovascular deconditioning. Additionally, in future studies, our model can be used in order to identify an optimal countermeasure strategy against spaceflight deconditioning by replicating the typical conditions encountered during exposure to lower body negative pressure – which, to date, shows conflicting and incongruent data about its effectiveness [93–95] – and artificial gravity [48].

CRediT authorship contribution statement

Francesco Tripoli: Writing – review & editing, Writing – original draft, Software, Methodology, Formal analysis, Conceptualization. **Luca Ridolfi:** Writing – review & editing, Supervision, Methodology, Formal analysis, Conceptualization. **Stefania Scarsoglio:** Writing – review & editing, Supervision, Methodology, Funding acquisition, Formal analysis, Conceptualization.

Funding sources

This study was carried out within the I-2022-05387 “Optimizing countermeasures against cardiovascular deconditioning and cerebral hemodynamics changes in long-term human spaceflights” project, which was selected via the Open Space Innovation Platform as a Co-Sponsored Research Agreement and carried out under the Discovery programme of, and funded by, the European Space Agency, France (contract number: 4000141523). This manuscript reflects only the authors’ views and opinions and the European Space Agency cannot be considered responsible for them.

Declaration of competing interest

The authors declare that they have no known competing financial interests or personal relationships that could have appeared to influence the work reported in this paper.

Acknowledgments

The authors would like to acknowledge the Discovery programme of the European Space Agency for funding this research.

Appendix A. Model validation of the central cardiovascular response

In this section, we briefly recall the validation of the cardiovascular model in the context of the central cardiac response to gravitational changes and, please, refer to our previous study [55] for further details. The cardiovascular model was validated against experimental data reported in centrifuge and parabolic flight studies (assessing both standing and seated posture). Specifically, in order to validate the model, the following variables were considered: heart rate (HR), stroke volume (SV), cardiac output (CO), mean arterial pressure (MAP), systolic arterial pressure (SAP), and diastolic arterial pressure (DAP).

After normalizing all variables with respect to the normo-gravity condition (1g), experimental data were pooled following the same approach described in Section 3.1. Additionally, for each investigated cardiac parameter, a linear regression was performed on measured data by means of the weighted least-squares fitting method, taking into account both pooled mean ($\mu^p_{X_j}$) and standard deviation ($\sigma^p_{X_j}$) values. Furthermore, for each regression line, statistical significance was verified by a two-sided t-test for the slope coefficient.

In Fig. A.6, the model results (solid black curves), the regression lines (dashed black lines), and the centrifuge (magenta lines) and parabolic flight (blue and green lines) data in terms of $\mu^p_{X_j}$ and $\sigma^p_{X_j}$ are shown. The linear regression analysis revealed that the trends in SV, HR, MAP, SAP, and DAP were statistically significant, whereas CO exhibited a p-value higher than the significance level of 0.05. Our cardiovascular model returned values that were in good agreement with the experimental data, with all model outcomes falling within the range $\mu^p_{X_j} \pm \sigma^p_{X_j}$, indicating that the model was able to capture the cardiovascular response to gravity changes in both micro- and hyper-gravity conditions. Specifically, SV exhibited a decreasing trend as a function of g, due to the fluid shift from the upper to the lower region (experimental data revealed a decrease between −29.8% and −39.5% from 0g to 2g, whereas the model predicted a reduction of −60.8% at 3g). HR increased due to the short-term regulation mechanisms (+57% from 0g to 2.5g in centrifuge studies, +33% and +12.8% from 0g to 1.8g in parabolic flights), resulting in a slightly decreasing CO (recall $CO = SV \cdot HR$). Due to baroreceptors, the model predicted a near-constant MAP throughout the investigated gravity range (whereas experimental data showed a mild increase). Finally, the model was able to capture the increase in diastolic pressure as a function of g, whereas some discrepancies were observed with the experimental data for SAP, with the model detecting a non-monotonic decrease as gravity increases from 0g to 3g. However, experimental data presented some incongruence and a decline in SAP was also detected during the hyper-gravity phase of parabolic flight in a standing posture.

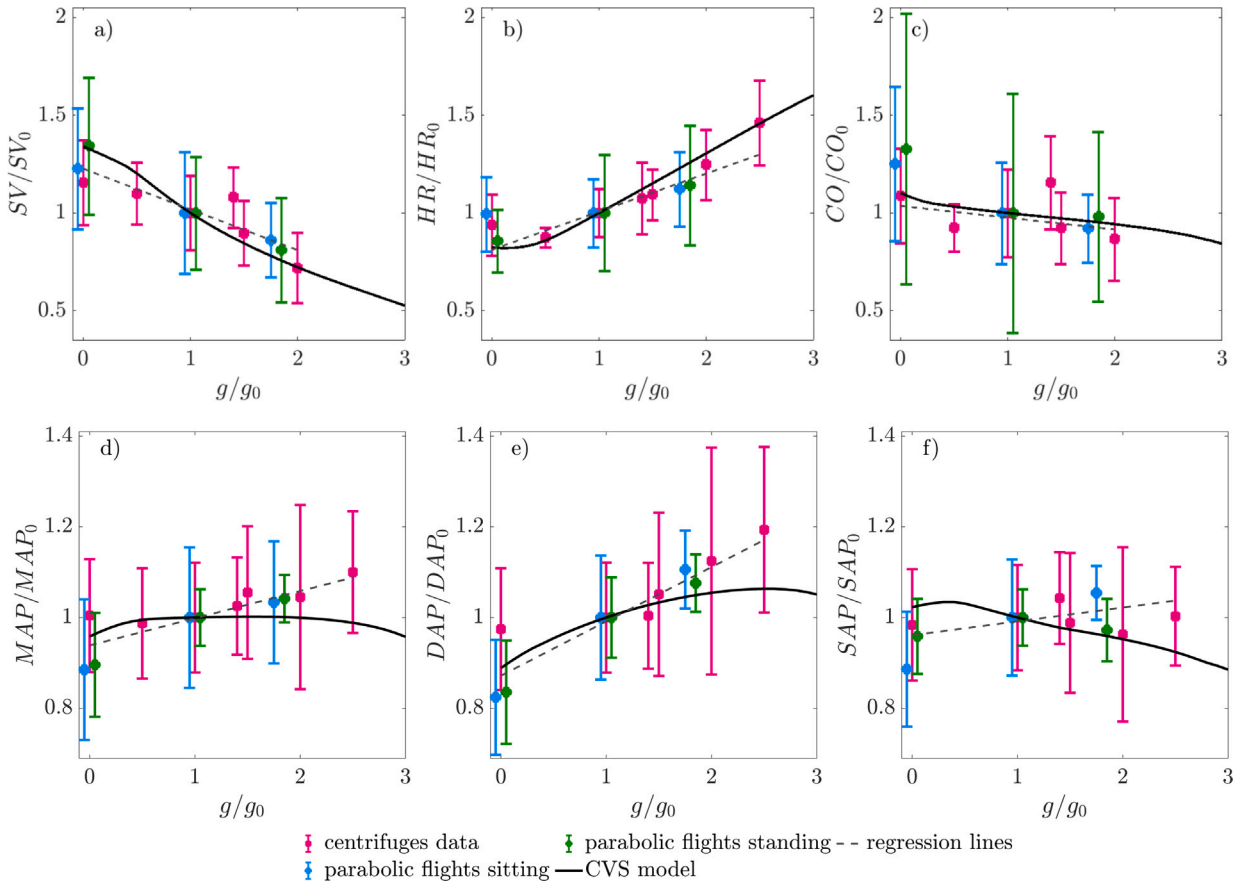

Fig. A.6. Pooled mean $\mu^p_{X_j}$ and standard deviation $\sigma^p_{X_j}$ values are depicted with vertical magenta (centrifuges data), blue (parabolic flights data in sitting posture), and green (parabolic flights data in standing posture) points and lines. Model outcomes and regression lines are depicted with black solid and dashed curves, respectively. Trends in SV (p-value < 0.001), HR (p-value < 0.001), MAP (p-value < 0.001), SAP (p-value = 0.0161), and DAP (p-value < 0.001) were statistically significant, whereas CO failed to pass the t-test with a p-value equal to 0.130. (For interpretation of the references to color in this figure legend, the reader is referred to the web version of this article.)

Appendix B. Supplementary data

Supplementary material related to this article can be found online at https://doi.org/10.1016/j.actaastro.2025.08.028.

References

[1] C.G. Blomqvist, H.L. Stone, Cardiovascular adjustments to gravitational stress, in: Comprehensive Physiology, Wiley, 1983, pp. 1025–1063, http://dx.doi.org/10.1002/cphy.cp020328, URL https://onlinelibrary.wiley.com/doi/10.1002/cphy.cp020328.

[2] H. Nocke, F. Meyer, V. Lessmann, Flow down gradients: the problem of pressure in this physiology core concept, Adv. Physiol. Ed. 47 (2023) 461–475, http://dx.doi.org/10.1152/advan.00107.2022, URL https://journals.physiology.org/doi/10.1152/advan.00107.2022.

[3] J.C. Buckey, F.A. Gaffney, L.D. Lane, B.D. Levine, D.E. Watenpaugh, S.J. Wright, C.W. Yancy, D.M. Meyer, C.G. Blomqvist, Central venous pressure in space, J. Appl. Physiol. 81 (1996) 19–25, http://dx.doi.org/10.1152/jappl.1996.81.1.19, URL https://www.physiology.org/doi/10.1152/jappl.1996.81.1.19.

[4] R. Videbaek, P. Norsk, Atrial distension in humans during microgravity induced by parabolic flights, J. Appl. Physiol. 83 (1997) 1862–1866, http://dx.doi.org/10.1152/jappl.1997.83.6.1862, URL https://www.physiology.org/doi/10.1152/jappl.1997.83.6.1862.

[5] G.C. Demontis, M.M. Germani, E.G. Caiani, I. Barravecchia, C. Passino, D. Angeloni, Human pathophysiological adaptations to the space environment, Front. Physiol. 8 (2017) http://dx.doi.org/10.3389/fphys.2017.00547, URL http://journal.frontiersin.org/article/10.3389/fphys.2017.00547/full.

[6] P. Norsk, Adaptation of the cardiovascular system to weightlessness: Surprises, paradoxes and implications for deep space missions, Acta Physiol. 228 (2020) http://dx.doi.org/10.1111/apha.13434, URL https://onlinelibrary.wiley.com/doi/10.1111/apha.13434.

[7] S.K. Arvedsen, O. Eiken, R. Kölegård, L.G. Petersen, P. Norsk, M. Damgaard, Body height and arterial pressure in seated and supine young males during +2 G centrifugation, Am. J. Physiology-Regulatory Integr. Comp. Physiol. 309 (2015) R1172–R1177, http://dx.doi.org/10.1152/ajpregu.00524.2014, URL https://www.physiology.org/doi/10.1152/ajpregu.00524.2014.

[8] O. Manen, C. Dussault, F. Sauvet, S. Montmerle-Borgdorff, Limitations of stroke volume estimation by non-invasive blood pressure monitoring in hypergravity, in: K. Jeyaseelan (Ed.), PLoS One 10 (2015) e0121936, http://dx.doi.org/10.1371/journal.pone.0121936, URL https://dx.plos.org/10.1371/journal.pone.0121936.

[9] J.C. Buckey, Space Physiology, Oxford University PressNew York, NY, 2006, http://dx.doi.org/10.1093/oso/9780195137255.001.0001, URL https://academic.oup.com/book/50937.

[10] E. Blaber, H. Marçal, B.P. Burns, Bioastronautics: The influence of microgravity on astronaut health, Astrobiology 10 (2010) 463–473, http://dx.doi.org/10.1089/ast.2009.0415, URL http://www.liebertpub.com/doi/10.1089/ast.2009.0415.

[11] G. Clément, Fundamentals of Space Medicine, Springer New York, New York, NY, 2011, http://dx.doi.org/10.1007/978-1-4419-9905-4, URL http://link.springer.com/10.1007/978-1-4419-9905-4.

[12] H.C. Gunga, Human physiology in extreme environments, Elsevier, 2015, pp. 1–320, http://dx.doi.org/10.1016/C2010-0-66676-4, URL https://linkinghub.elsevier.com/retrieve/pii/C20100666764,

[13] L.R. Young, J.P. Sutton (Eds.), Handbook of Bioastronautics, Springer International Publishing, Cham, 2021, http://dx.doi.org/10.1007/978-3-319-12191-8, URL https://link.springer.com/10.1007/978-3-319-12191-8.

[14] N. Goswami, O. White, A. Blaber, J. Evans, J.J. van Loon, G. Clement, Human physiology adaptation to altered gravity environments, Acta Astronaut. 189 (2021) 216–221, http://dx.doi.org/10.1016/j.actaastro.2021.08.023, URL https://linkinghub.elsevier.com/retrieve/pii/S0094576521004434.

[15] P. Arbeille, G. Fomina, J. Roumy, I. Alferova, N. Tobal, S. Herault, Adaptation of the left heart, cerebral and femoral arteries, and jugular and femoral veins during short- and long-term head-down tilt and spaceflights, Eur. J. Appl. Physiol. 86 (2001) 157–168, http://dx.doi.org/10.1007/s004210100473, URL http://link.springer.com/10.1007/s004210100473.

[16] E.G. Caiani, L. Sugeng, L. Weinert, A. Capderou, R.M. Lang, P. Vaïda, Objective evaluation of changes in left ventricular and atrial volumes during parabolic flight using real-time three-dimensional echocardiography, J. Appl. Physiol. 101 (2006) 460–468, http://dx.doi.org/10.1152/japplphysiol.00014.2006, URL https://www.physiology.org/doi/10.1152/japplphysiol.00014.2006.

[17] A.R. Hargens, S. Richardson, Cardiovascular adaptations, fluid shifts, and countermeasures related to space flight, Respir. Physiol. Neurobiol. 169 (2009) S30–S33, http://dx.doi.org/10.1016/j.resp.2009.07.005, URL https://linkinghub.elsevier.com/retrieve/pii/S1569904809001840.

[18] A. Grigoriev, A. Kotovskaya, G. Fomina, The human cardiovascular system during space flight, Acta Astronaut. 68 (2011) 1495–1500, http://dx.doi.org/10.1016/j.actaastro.2009.11.013, URL https://linkinghub.elsevier.com/retrieve/pii/S0094576509005633.

[19] J. Du, J. Cui, J. Yang, P. Wang, L. Zhang, B. Luo, B. Han, Alterations in cerebral hemodynamics during microgravity: A literature review, Med. Sci. Monit. 27 (2021) http://dx.doi.org/10.12659/MSM.928108, URL https://www.medscimonit.com/abstract/index/idArt/928108.

[20] R.D. Seidler, C. Stern, M. Basner, A.C. Stahn, F.L. Wuyts, P. zu Eulenburg, Future research directions to identify risks and mitigation strategies for neurostructural, ocular, and behavioral changes induced by human spaceflight: A NASA-ESA expert group consensus report, Front. Neural Circuits 16 (2022) http://dx.doi.org/10.3389/fncir.2022.876789, URL https://www.frontiersin.org/articles/10.3389/fncir.2022.876789/full.

[21] T.H. Mader, C.R. Gibson, A.F. Pass, L.A. Kramer, A.G. Lee, J. Fogarty, W.J. Tarver, J.P. Dervay, D.R. Hamilton, A. Sargsyan, J.L. Phillips, D. Tran, W. Lipsky, J. Choi, C. Stern, R. Kuyumjian, J.D. Polk, Optic disc edema, globe flattening, choroidal folds, and hyperopic shifts observed in astronauts after long-duration space flight, Ophthalmology 118 (2011) 2058–2069, http://dx.doi.org/10.1016/j.ophtha.2011.06.021, URL https://linkinghub.elsevier.com/retrieve/pii/S0161642011005641.

[22] J.P. Berdahl, D.Y. Yu, W.H. Morgan, The translaminar pressure gradient in sustained zero gravity, idiopathic intracranial hypertension, and glaucoma, Med. Hypotheses 79 (2012) 719–724, http://dx.doi.org/10.1016/j.mehy.2012.08.009, URL https://linkinghub.elsevier.com/retrieve/pii/S0306987712003763.

[23] S.S. Laurie, G. Vizzeri, G. Taibbi, C.R. Ferguson, X. Hu, S.M.C. Lee, R. Ploutz-Snyder, S.M. Smith, S.R. Zwart, M.B. Stenger, Effects of short-term mild hypercapnia during head-down tilt on intracranial pressure and ocular structures in healthy human subjects, Physiol. Rep. 5 (2017) http://dx.doi.org/10.14814/phy2.13302, URL https://onlinelibrary.wiley.com/doi/10.14814/phy2.13302.

[24] A.G. Lee, T.H. Mader, C.R. Gibson, T.J. Brunstetter, W.J. Tarver, Space flight-associated neuro-ocular syndrome (SANS), Eye 32 (2018) 1164–1167, http://dx.doi.org/10.1038/s41433-018-0070-y, URL https://www.nature.com/articles/s41433-018-0070-y.

[25] A.G. Lee, T.H. Mader, C.R. Gibson, W. Tarver, P. Rabiei, R.F. Riascos, L.A. Galdamez, T. Brunstetter, Spaceflight associated neuro-ocular syndrome (SANS) and the neuro-ophthalmologic effects of microgravity: a review and an update, Npj Microgravity 6 (2020) 7, http://dx.doi.org/10.1038/s41526-020-0097-9, URL https://www.nature.com/articles/s41526-020-0097-9.

[26] C. Stern, Y.H. Yücel, P. zu Eulenburg, A.P.-L. Traon, L.G. Petersen, Eye-brain axis in microgravity and its implications for spaceflight associated neuro-ocular syndrome, Npj Microgravity 9 (2023) 56, http://dx.doi.org/10.1038/s41526-023-00300-4, URL https://www.nature.com/articles/s41526-023-00300-4.

[27] J. Ong, W. Tarver, T. Brunstetter, T.H. Mader, C.R. Gibson, S.S. Mason, A. Lee, Spaceflight associated neuro-ocular syndrome: proposed pathogenesis, terrestrial analogues, and emerging countermeasures, Br. J. Ophthalmol. 107 (2023) 895–900, http://dx.doi.org/10.1136/bjo-2022-322892, URL https://bjo.bmj.com/lookup/doi/10.1136/bjo-2022-322892.

[28] M.M. Solano, R. Dumas, M.R. Lesk, S. Costantino, Ocular biomechanical responses to long-duration spaceflight, IEEE Open J. Eng. Med. Biology 6 (2025) 127–132, http://dx.doi.org/10.1109/OJEMB.2024.3453049, URL https://ieeexplore.ieee.org/document/10666778/.

[29] Z.S. Patel, T.J. Brunstetter, W.J. Tarver, A.M. Whitmire, S.R. Zwart, S.M. Smith, J.L. Huff, Red risks for a journey to the red planet: The highest priority human health risks for a mission to Mars, Npj Microgravity 6 (2020) 33, http://dx.doi.org/10.1038/s41526-020-00124-6, URL https://www.nature.com/articles/s41526-020-00124-6.

[30] K. Marshall-Bowman, M.R. Barratt, C.R. Gibson, Ophthalmic changes and increased intracranial pressure associated with long duration spaceflight: An emerging understanding, Acta Astronaut. 87 (2013) 77–87, http://dx.doi.org/10.1016/j.actaastro.2013.01.014, URL https://linkinghub.elsevier.com/retrieve/pii/S009457651300026X.

[31] G. Taibbi, R.L. Cromwell, K.G. Kapoor, B.F. Godley, G. Vizzeri, The effect of microgravity on ocular structures and visual function: A review, Surv. Ophthalmol. 58 (2013) 155–163, http://dx.doi.org/10.1016/j.survophthal.2012.04.002, URL https://linkinghub.elsevier.com/retrieve/pii/S0039625712000951.

[32] L.-F. Zhang, A.R. Hargens, Spaceflight-induced intracranial hypertension and visual impairment: Pathophysiology and countermeasures, Physiol. Rev. 98 (2018) 59–87, http://dx.doi.org/10.1152/physrev.00017.2016, URL https://www.physiology.org/doi/10.1152/physrev.00017.2016.

[33] A.S. Huang, M.B. Stenger, B.R. Macias, Gravitational influence on intraocular pressure: Implications for spaceflight and disease, J. Glaucoma 28 (2019) 756–764, http://dx.doi.org/10.1097/IJG.0000000000001293, URL https://journals.lww.com/00061198-201908000-00015.

[34] J.S. Lawley, L.G. Petersen, E.J. Howden, S. Sarma, W.K. Cornwell, R. Zhang, L.A. Whitworth, M.A. Williams, B.D. Levine, Effect of gravity and microgravity on intracranial pressure, J. Physiol. 595 (2017) 2115–2127, http://dx.doi.org/10.1113/JP273557, URL https://physoc.onlinelibrary.wiley.com/doi/10.1113/JP273557.

[35] K. Marshall-Goebel, E. Mulder, E. Bershad, C. Laing, A. Eklund, J. Malm, C. Stern, J. Rittweger, Intracranial and intraocular pressure during various degrees of head-down tilt, Aerosp. Med. Hum. Perform. 88 (2017) 10–16, http://dx.doi.org/10.3357/AMHP.4653.2017, URL https://asma.kglmeridian.com/view/journals/amhp/88/1/article-p10.xml.

[36] A.P.-L. Traon, M. Heer, M.V. Narici, J. Rittweger, J. Vernikos, From space to earth: advances in human physiology from 20 years of bed rest studies (1986–2006), Eur. J. Appl. Physiol. 101 (2007) 143–194, http://dx.doi.org/10.1007/s00421-007-0474-z, URL http://link.springer.com/10.1007/s00421-007-0474-z.

[37] A. Saveko, M. Bekreneva, I. Ponomarev, I. Zelenskaya, A. Riabova, T. Shigueva, V. Kitov, N.A. Sheli, I. Nosikova, I. Rukavishnikov, D. Sayenko, E. Tomilovskaya, Impact of different ground-based microgravity models on human sensorimotor system, Front. Physiol. 14 (2023) 1085545, http://dx.doi.org/10.3389/fphys.2023.1085545, URL https://www.frontiersin.org/articles/10.3389/fphys.2023.1085545/full.

[38] F. Karmali, M. Shelhamer, The dynamics of parabolic flight: Flight characteristics and passenger percepts, Acta Astronaut. 63 (2008) 594–602, http://dx.doi.org/10.1016/j.actaastro.2008.04.009, URL https://linkinghub.elsevier.com/retrieve/pii/S0094576508001574.

[39] N. Goswami, M. Bruner, D. Xu, M.-P. Bareille, A. Beck, H. Hinghofer-Szalkay, A.P. Blaber, Short-arm human centrifugation with 0.4g at eye and 0.75g at heart level provides similar cerebrovascular and cardiovascular responses to standing, Eur. J. Appl. Physiol. 115 (2015) 1569–1575, http://dx.doi.org/10.1007/s00421-015-3142-8, URL http://link.springer.com/10.1007/s00421-015-3142-8.

[40] H. Habazettl, A. Stahn, A. Nitsche, M. Nordine, A.R. Pries, H.C. Gunga, O. Opatz, Microvascular responses to (hyper-)gravitational stress by short-arm human centrifuge: arteriolar vasoconstriction and venous pooling, Eur. J. Appl. Physiol. 116 (2016) 57–65, http://dx.doi.org/10.1007/s00421-015-3241-6, URL http://link.springer.com/10.1007/s00421-015-3241-6.

[41] S. Ogoh, A. Hirasawa, P.B. Raven, T. Rebuffat, P. Denise, R. Lericollais, J. Sugawara, H. Normand, Effect of an acute increase in central blood volume on cerebral hemodynamics, Am. J. Physiology-Regulatory Integr. Comp. Physiol. 309 (2015) R902–R911, http://dx.doi.org/10.1152/ajpregu.00137.2015, URL https://www.physiology.org/doi/10.1152/ajpregu.00137.2015.

[42] T. Klein, M. Sanders, P. Wollseiffen, H. Carnahan, V. Abeln, C.D. Askew, J.A. Claassen, S. Schneider, Transient cerebral blood flow responses during microgravity, Life Sci. Space Res. 25 (2020) 66–71, http://dx.doi.org/10.1016/j.lssr.2020.03.003, URL https://linkinghub.elsevier.com/retrieve/pii/S221455242030016X.

[43] S. Schneider, V. Abeln, C.D. Askew, T. Vogt, U. Hoffmann, P. Denise, H.K. Strüder, Changes in cerebral oxygenation during parabolic flight, Eur. J. Appl. Physiol. 113 (2013) 1617–1623, http://dx.doi.org/10.1007/s00421-013-2588-9, URL http://link.springer.com/10.1007/s00421-013-2588-9.

[44] Y. Ogawa, R. Yanagida, K. Ueda, K. Aoki, K. ichi Iwasaki, The relationship between widespread changes in gravity and cerebral blood flow, Environ. Heal. Prev. Med. 21 (2016) 186–192, http://dx.doi.org/10.1007/s12199-016-0513-7, URL http://link.springer.com/10.1007/s12199-016-0513-7.

[45] T. Konishi, T. Kurazumi, T. Kato, C. Takko, Y. Ogawa, K. ichi Iwasaki, Changes in cerebral oxygen saturation and cerebral blood flow velocity under mild +Gz hypergravity, J. Appl. Physiol. 127 (2019) 190–197, http://dx.doi.org/10.1152/japplphysiol.00119.2019, URL https://www.physiology.org/doi/10.1152/japplphysiol.00119.2019.

[46] D.G. Newman, R. Callister, Cardiovascular training effects in fighter pilots induced by occupational high G exposure, Aviat. Space Environ. Med. 79 (2008) 774–778, http://dx.doi.org/10.3357/ASEM.1575.2008, URL https://asma.kglmeridian.com/view//journals/asem/79/8/article-p774.xml.

[47] S. Lalande, F. Buick, Physiologic +Gz tolerance responses over successive +Gz exposures in simulated air combat maneuvers, Aviat. Space Environ. Med. 80 (2009) 1032–1038, http://dx.doi.org/10.3357/ASEM.2525.2009, URL https://asma.kglmeridian.com/view//journals/asem/80/12/article-p1032.xml.

[48] G.R. Clément, A.P. Bukley, W.H. Paloski, Artificial gravity as a countermeasure for mitigating physiological deconditioning during long-duration space missions, Front. Syst. Neurosci. 9 (2015) 92, http://dx.doi.org/10.3389/fnsys.2015.00092, URL http://journal.frontiersin.org/Article/10.3389/fnsys.2015.00092/abstract.

[49] T. Heldt, E.B. Shim, R.D. Kamm, R.G. Mark, Computational modeling of cardiovascular response to orthostatic stress, J. Appl. Physiol. 92 (2002) 1239–1254, http://dx.doi.org/10.1152/japplphysiol.00241.2001, URL https://www.physiology.org/doi/10.1152/japplphysiol.00241.2001.

[50] A. Diaz-Artiles, T. Heldt, L.R. Young, Computational model of cardiovascular response to centrifugation and lower body cycling exercise, J. Appl. Physiol. 127 (2019) 1453–1468, http://dx.doi.org/10.1152/japplphysiol.00314.2019, URL https://www.physiology.org/doi/10.1152/japplphysiol.00314.2019.

[51] C. Gallo, L. Ridolfi, S. Scarsoglio, Cardiovascular deconditioning during long-term spaceflight through multiscale modeling, Npj Microgravity 6 (2020) 27, http://dx.doi.org/10.1038/s41526-020-00117-5, URL https://www.nature.com/articles/s41526-020-00117-5.

[52] R.S. Whittle, A. Diaz-Artiles, Modeling individual differences in cardiovascular response to gravitational stress using a sensitivity analysis, J. Appl. Physiol. 130 (2021) 1983–2001, http://dx.doi.org/10.1152/japplphysiol.00727.2020, URL https://journals.physiology.org/doi/10.1152/japplphysiol.00727.2020.

[53] P. Holmlund, K.-H. Støverud, A. Eklund, Mathematical modelling of the CSF system: effects of microstructures and posture on optic nerve subarachnoid space dynamics, Fluids Barriers the CNS 19 (2022) 67, http://dx.doi.org/10.1186/s12987-022-00366-4, URL https://fluidsbarrierscns.biomedcentral.com/articles/10.1186/s12987-022-00366-4.

[54] M. Fois, A. Diaz-Artiles, S.Y. Zaman, L. Ridolfi, S. Scarsoglio, Linking cerebral hemodynamics and ocular microgravity-induced alterations through an in silico-in vivo head-down tilt framework, Npj Microgravity 10 (2024) 22, http://dx.doi.org/10.1038/s41526-024-00366-8, URL https://www.nature.com/articles/s41526-024-00366-8.

[55] F. Tripoli, L. Ridolfi, S. Scarsoglio, Assessing the cardiac function from microgravity to hyper-gravity conditions through a validated multiscale modelling approach, J. Physiol. (2025) http://dx.doi.org/10.1113/JP287142, URL https://physoc.onlinelibrary.wiley.com/doi/10.1113/JP287142.

[56] F. Tripoli, L. Ridolfi, S. Scarsoglio, Acute cardiovascular response to gravity changes: A multiscale mathematical model for microgravity and hypergravity applications, in: IAF/IAA Space Life Sciences Symposium, International Astronautical Federation (IAF), Paris, France, 2024, pp. 1106–1117, http://dx.doi.org/10.52202/078355-0132, URL http://www.proceedings.com/078355-0132.html.

[57] P. Holmlund, A. Eklund, L.-O.D. Koskinen, E. Johansson, N. Sundström, J. Malm, S. Qvarlander, Venous collapse regulates intracranial pressure in upright body positions, Am. J. Physiology-Regulatory Integr. Comp. Physiol. 314 (2018) R377–R385, http://dx.doi.org/10.1152/ajpregu.00291.2017, URL https://www.physiology.org/doi/10.1152/ajpregu.00291.2017.

[58] M. Fois, S.V. Maule, M. Giudici, M. Valente, L. Ridolfi, S. Scarsoglio, Cardiovascular response to posture changes: Multiscale modeling and in vivo validation during head-up tilt, Front. Physiol. 13 (2022) 826989, http://dx.doi.org/10.3389/fphys.2022.826989, URL https://www.frontiersin.org/articles/10.3389/fphys.2022.826989/full.

[59] A.P. Anderson, J.G. Swan, S.D. Phillips, D.A. Knaus, N.T. Kattamis, C.M. Toutain-Kidd, M.E. Zegans, A.M. Fellows, J.C. Buckey, Acute effects of changes to the gravitational vector on the eye, J. Appl. Physiol. 120 (2016) 939–946, http://dx.doi.org/10.1152/japplphysiol.00730.2015, URL https://www.physiology.org/doi/10.1152/japplphysiol.00730.2015.

[60] B.J. Linder, G.L. Trick, M.L. Wolf, Altering body position affects intraocular pressure and visual function., Investig. Ophthalmol. Vis. Sci. 29 (1988) 1492–1497, URL http://www.ncbi.nlm.nih.gov/pubmed/3170121.

[61] X. Zhang, J.E. Medow, B.J. Iskandar, F. Wang, M. Shokoueinejad, J. Koueik, J.G. Webster, Invasive and noninvasive means of measuring intracranial pressure: a review, Physiol. Meas. 38 (2017) R143–R182, http://dx.doi.org/10.1088/1361-6579/aa7256, URL https://iopscience.iop.org/article/10.1088/1361-6579/aa7256.

[62] F.D. Silva, M. Lira, Intraocular pressure measurement: A review, Surv. Ophthalmol. 67 (2022) 1319–1331, http://dx.doi.org/10.1016/j.survophthal.2022.03.001, URL https://linkinghub.elsevier.com/retrieve/pii/S0039625722000388.

[63] M. Borenstein, L.V. Hedges, J.P.T. Higgins, H.R. Rothstein, Introduction to Meta-Analysis, Wiley, 2009, http://dx.doi.org/10.1002/9780470743386, URL https://onlinelibrary.wiley.com/doi/book/10.1002/9780470743386.

[64] A.F. Folino, Cerebral autoregulation and syncope, Prog. Cardiovasc. Dis. 50 (2007) 49–80, http://dx.doi.org/10.1016/j.pcad.2007.01.001, URL https://linkinghub.elsevier.com/retrieve/pii/S0033062007000023.

[65] A.P. Blaber, K.A. Zuj, N. Goswami, Cerebrovascular autoregulation: lessons learned from spaceflight research, Eur. J. Appl. Physiol. 113 (2013) 1909–1917, http://dx.doi.org/10.1007/s00421-012-2539-x, URL http://link.springer.com/10.1007/s00421-012-2539-x.

[66] S. Scarsoglio, M. Fois, L. Ridolfi, Increased hemodynamic pulsatility in the cerebral microcirculation during parabolic flight-induced microgravity: A computational investigation, Acta Astronaut. 211 (2023) 344–352, http://dx.doi.org/10.1016/j.actaastro.2023.06.018, URL https://linkinghub.elsevier.com/retrieve/pii/S009457652300317X.

[67] S. Scarsoglio, A. Saglietto, M. Anselmino, F. Gaita, L. Ridolfi, Alteration of cerebrovascular haemodynamic patterns due to atrial fibrillation: an in silico investigation, J. R. Soc. Interface 14 (2017) 20170180, http://dx.doi.org/10.1098/rsif.2017.0180, URL https://royalsocietypublishing.org/doi/10.1098/rsif.2017.0180.

[68] E.S. Nelson, L. Mulugeta, A. Feola, J. Raykin, J.G. Myers, B.C. Samuels, C.R. Ethier, The impact of ocular hemodynamics and intracranial pressure on intraocular pressure during acute gravitational changes, J. Appl. Physiol. 123 (2017) 352–363, http://dx.doi.org/10.1152/japplphysiol.00102.2017, URL https://www.physiology.org/doi/10.1152/japplphysiol.00102.2017.

[69] M. Shen, W.H. Frishman, Effects of spaceflight on cardiovascular physiology and health, Cardiol. Rev. 27 (2019) 122–126, http://dx.doi.org/10.1097/CRD.0000000000000236, URL https://journals.lww.com/00045415-201905000-00002.

[70] P. Holmlund, E. Johansson, S. Qvarlander, A. Wåhlin, K. Ambarki, L.-O.D. Koskinen, J. Malm, A. Eklund, Human jugular vein collapse in the upright posture: implications for postural intracranial pressure regulation, Fluids Barriers the CNS 14 (2017) 17, http://dx.doi.org/10.1186/s12987-017-0065-2, URL http://fluidsbarrierscns.biomedcentral.com/articles/10.1186/s12987-017-0065-2.

[71] Y. Shi, M.J. Thrippleton, G.W. Blair, D.A. Dickie, I. Marshall, I. Hamilton, F.N. Doubal, F. Chappell, J.M. Wardlaw, Small vessel disease is associated with altered cerebrovascular pulsatility but not resting cerebral blood flow, J. Cereb. Blood Flow Metab. 40 (2020) 85–99, http://dx.doi.org/10.1177/0271678X18803956, URL https://journals.sagepub.com/doi/10.1177/0271678X18803956.

[72] C.-P. Chung, H.-Y. Lee, P.-C. Lin, P.-N. Wang, Cerebral artery pulsatility is associated with cognitive impairment and predicts dementia in individuals with subjective memory decline or mild cognitive impairment, in: S. Salmerón (Ed.), J. Alzheimer's Dis. 60 (2017) 625–632, http://dx.doi.org/10.3233/JAD-170349, URL https://journals.sagepub.com/doi/10.3233/JAD-170349.

[73] D.M. Bailey, D. Lanéelle, J.-E. Trihan, N. Marchi, B.S. Stacey, K. Tamiya, T. Washio, E. Tuaillon, C. Hirtz, S. Lehmann, S. Ogoh, H. Normand, Gravitational transitions increase posterior cerebral perfusion and systemic oxidative-nitrosative stress: Implications for neurovascular unit integrity, Neuroscience 441 (2020) 142–160, http://dx.doi.org/10.1016/j.neuroscience.2020.05.048, URL https://linkinghub.elsevier.com/retrieve/pii/S030645222030350X.

[74] S. Ogoh, K. Sato, K. Okazaki, T. Miyamoto, A. Hirasawa, T. Sadamoto, M. Shibasaki, Blood flow in internal carotid and vertebral arteries during graded lower body negative pressure in humans, Exp. Physiol. 100 (2015) 259–266, http://dx.doi.org/10.1113/expphysiol.2014.083964, URL https://physoc.onlinelibrary.wiley.com/doi/10.1113/expphysiol.2014.083964.

[75] K. Sato, J.P. Fisher, T. Seifert, M. Overgaard, N.H. Secher, S. Ogoh, Blood flow in internal carotid and vertebral arteries during orthostatic stress, Exp. Physiol. 97 (2012) 1272–1280, http://dx.doi.org/10.1113/expphysiol.2012.064774, URL https://physoc.onlinelibrary.wiley.com/doi/10.1113/expphysiol.2012.064774.

[76] L. Tatu, T. Moulin, J. Bogousslavsky, H. Duvernoy, Arterial territories of human brain, Neurology 47 (1996) 1125–1135, http://dx.doi.org/10.1212/WNL.47.5.1125, URL https://www.neurology.org/doi/10.1212/WNL.47.5.1125.

[77] B.M. Deegan, J.P. Cooke, D. Lyons, G. OLaighin, J.M. Serrador, Cerebral autoregulation in the vertebral and middle cerebral arteries during combine head upright tilt and lower body negative pressure in healthy humans, in: 2010 Annual International Conference of the IEEE Engineering in Medicine and Biology, IEEE, 2010, pp. 2505–2508, http://dx.doi.org/10.1109/IEMBS.2010.5626647, URL http://ieeexplore.ieee.org/document/5626647/.

[78] M.M. Tymko, C.A. Rickards, R.J. Skow, N.C. Ingram-Cotton, M.K. Howatt, T.A. Day, The effects of superimposed tilt and lower body negative pressure on anterior and posterior cerebral circulations, Physiol. Rep. 4 (2016) e12957, http://dx.doi.org/10.14814/phy2.12957, URL http://doi.wiley.com/10.14814/phy2.12957.

[79] J. Kaur, J.R. Vranish, T.C. Barbosa, T. Washio, B.E. Young, B.Y. Stephens, R.M. Brothers, S. Ogoh, P.J. Fadel, Regulation of regional cerebral blood flow during graded reflex-mediated sympathetic activation via lower body negative pressure, J. Appl. Physiol. 125 (2018) 1779–1786, http://dx.doi.org/10.1152/japplphysiol.00623.2018, URL https://www.physiology.org/doi/10.1152/japplphysiol.00623.2018.

[80] R. Zhang, J.H. Zuckerman, B.D. Levine, Deterioration of cerebral autoregulation during orthostatic stress: insights from the frequency domain, J. Appl. Physiol. 85 (1998) 1113–1122, http://dx.doi.org/10.1152/jappl.1998.85.3.1113, URL https://www.physiology.org/doi/10.1152/jappl.1998.85.3.1113.

[81] K.A. Zuj, P. Arbeille, J.K. Shoemaker, A.P. Blaber, D.K. Greaves, D. Xu, R.L. Hughson, Impaired cerebrovascular autoregulation and reduced CO^2 reactivity after long duration spaceflight, Am. J. Physiology-Heart Circ. Physiol. 302 (2012) H2592–H2598, http://dx.doi.org/10.1152/ajpheart.00029.2012, URL https://www.physiology.org/doi/10.1152/ajpheart.00029.2012.

[82] L.G. Petersen, R.S. Whittle, J.H. Lee, J. Sieker, J. Carlson, C. Finke, C.M. Shelton, J.C.G. Petersen, A. Diaz-Artiles, Gravitational effects on intraocular pressure and ocular perfusion pressure, J. Appl. Physiol. 132 (2022) 24–35, http://dx.doi.org/10.1152/japplphysiol.00546.2021, URL https://journals.physiology.org/doi/10.1152/japplphysiol.00546.2021.

[83] S. Ogoh, T. Washio, J.F.R. Paton, J.P. Fisher, L.G. Petersen, Gravitational effects on intracranial pressure and blood flow regulation in young men: a potential shunting role for the external carotid artery, J. Appl. Physiol. 129 (2020) 901–908, http://dx.doi.org/10.1152/japplphysiol.00369.2020, URL https://journals.physiology.org/doi/10.1152/japplphysiol.00369.2020.

[84] P.K. Eide, M. Sroka, A. Wozniak, T. Sæhle, Morphological characterization of cardiac induced intracranial pressure (ICP) waves in patients with overdrainage of cerebrospinal fluid and negative ICP, Med. Eng. Phys. 34 (2012) 1066–1070, http://dx.doi.org/10.1016/j.medengphy.2011.11.011, URL https://linkinghub.elsevier.com/retrieve/pii/S135045331100302X.

[85] J.P. Berdahl, R.R. Allingham, Intracranial pressure and glaucoma, Curr. Opin. Ophthalmol. 21 (2010) 106–111, http://dx.doi.org/10.1097/ICU.0b013e32833651d8, URL http://journals.lww.com/00055735-201003000-00004.

[86] T.J. McCulley, J.R. Chang, W.J. Piluek, Intracranial pressure and glaucoma, J. Neuro-Ophthalmology 35 (2015) S38–S44, http://dx.doi.org/10.1097/WNO.0000000000000295, URL https://journals.lww.com/00041327-201509001-00006.

[87] A.J. Baneke, J. Aubry, A.C. Viswanathan, G.T. Plant, The role of intracranial pressure in glaucoma and therapeutic implications, Eye 34 (2020) 178–191, http://dx.doi.org/10.1038/s41433-019-0681-y, URL https://www.nature.com/articles/s41433-019-0681-y.

[88] D.A. Price, A. Harris, B. Siesky, S. Mathew, The influence of translaminar pressure gradient and intracranial pressure in glaucoma: A review, J. Glaucoma 29 (2020) 141–146, http://dx.doi.org/10.1097/IJG.0000000000001421, URL https://journals.lww.com/10.1097/IJG.0000000000001421.

[89] D. Schmidl, G. Garhofer, L. Schmetterer, The complex interaction between ocular perfusion pressure and ocular blood flow – Relevance for glaucoma, Exp. Eye Res. 93 (2011) 141–155, http://dx.doi.org/10.1016/j.exer.2010.09.002, URL https://linkinghub.elsevier.com/retrieve/pii/S0014483510002976.

[90] Z. He, A.J. Vingrys, J.A. Armitage, B.V. Bui, The role of blood pressure in glaucoma, Clin. Exp. Optom. 94 (2011) 133–149, http://dx.doi.org/10.1111/j.1444-0938.2010.00564.x, URL https://www.tandfonline.com/doi/full/10.1111/j.1444-0938.2010.00564.x.

[91] M. Ursino, M. Giannessi, A model of cerebrovascular reactivity including the circle of willis and cortical anastomoses, Ann. Biomed. Eng. 38 (2010) 955–974, http://dx.doi.org/10.1007/s10439-010-9923-7, URL http://link.springer.com/10.1007/s10439-010-9923-7.

[92] V. Novak, J.M. Spies, P. Novak, B.R. McPhee, T.A. Rummans, P.A. Low, Hypocapnia and cerebral hypoperfusion in orthostatic intolerance, Stroke 29 (1998) 1876–1881, http://dx.doi.org/10.1161/01.STR.29.9.1876, URL https://www.ahajournals.org/doi/10.1161/01.STR.29.9.1876.

[93] L.G. Petersen, J.S. Lawley, A. Lilja-Cyron, J.C.G. Petersen, E.J. Howden, S. Sarma, W.K. Cornwell, R. Zhang, L.A. Whitworth, M.A. Williams, M. Juhler, B.D. Levine, Lower body negative pressure to safely reduce intracranial pressure, J. Physiol. 597 (2019) 237–248, http://dx.doi.org/10.1113/JP276557, URL https://physoc.onlinelibrary.wiley.com/doi/10.1113/JP276557.

[94] S.H. Greenwald, B.R. Macias, S.M.C. Lee, K. Marshall-Goebel, D.J. Ebert, J.H.K. Liu, R.J. Ploutz-Snyder, I.V. Alferova, S.A. Dulchavsky, A.R. Hargens, M.B. Stenger, S.S. Laurie, Intraocular pressure and choroidal thickness respond differently to lower body negative pressure during spaceflight, J. Appl. Physiol. 131 (2021) 613–620, http://dx.doi.org/10.1152/japplphysiol.01040.2020, URL https://journals.physiology.org/doi/10.1152/japplphysiol.01040.2020.

[95] E.A. Hall, R.S. Whittle, A. Diaz-Artiles, Ocular perfusion pressure is not reduced in response to lower body negative pressure, Npj Microgravity 10 (2024) 67, http://dx.doi.org/10.1038/s41526-024-00404-5, URL https://www.nature.com/articles/s41526-024-00404-5.

Francesco Tripoli is a Ph.D. student in Aerospace Engineering at Politecnico di Torino. He completed his M.Sc. in Biomedical Engineering at Politecnico di Torino in 2022. From October 2022 to October 2023, he received a post-graduate research scholarship at Politecnico di Torino. During this period, he applied numerical methods to investigate cerebral hemodynamics in atrial fibrillation. His current research focuses on both cardiovascular and cerebro-ocular functions under spaceflight conditions, exploiting mathematical multiscale modeling. His work aims to enhance the comprehension of cardiovascular and cerebral deconditioning during long-term human spaceflight and to support the identification of effective countermeasure strategies.

Luca Ridolfi is full professor in Hydraulics and Fluid Mechanics at the Politecnico di Torino. He was Department Head and coordinator of Ph.D. program in Civil and Environment Engineering. He was visiting professor at Texas A&M University and Princeton University. His research interests concern wall turbulence, hemodynamics, noise-induced phenomena, pattern formation, and network analysis.

Stefania Scarsoglio is full professor in Fluid Dynamics at the Politecnico di Torino. She has been visiting scholar at the University of Washington and Massachusetts Institute of Technology. Her research interests involve cardiovascular fluid dynamics and space medicine. In particular, her activities focus on the impact of cardiovascular diseases and extreme conditions on the cardiovascular system, by combining mathematical models, computational fluid dynamics and clinical measurements.